A genetic memory initiates the epigenetic loop necessary to preserve centromere position

Sebastian Hoffmann, Helena M Izquierdo, Riccardo Gamba, Florian Chardon, Marie Dumont, Veer Keizer, Solène Hervé, Shannon M Mcnulty, Beth A Sullivan, Nicolas Manel, et al.

Article

SOURCE DATA | TRANSPARENT PROCESS

THE EMBO JOURNAL

A genetic memory initiates the epigenetic loop necessary to preserve centromere position

Sebastian Hoffmann[1], Helena M Izquierdo[2,†], Riccardo Gamba[1,†], Florian Chardon[1], Marie Dumont[1], Veer Keizer[1], Solène Hervé[1], Shannon M McNulty[3], Beth A Sullivan[3], Nicolas Manel[2] & Daniele Fachinetti[1,*]

Abstract

Centromeres are built on repetitive DNA sequences (CenDNA) and a specific chromatin enriched with the histone H3 variant CENP-A, the epigenetic mark that identifies centromere position. Here, we interrogate the importance of CenDNA in centromere specification by developing a system to rapidly remove and reactivate CENP-A (CENP-A$^{OFF/ON}$). Using this system, we define the temporal cascade of events necessary to maintain centromere position. We unveil that CENP-B bound to CenDNA provides memory for maintenance on human centromeres by promoting *de novo* CENP-A deposition. Indeed, lack of CENP-B favors neocentromere formation under selective pressure. Occasionally, CENP-B triggers centromere re-activation initiated by CENP-C, but not CENP-A, recruitment at both ectopic and native centromeres. This is then sufficient to initiate the CENP-A-based epigenetic loop. Finally, we identify a population of CENP-A-negative, CENP-B/C-positive resting CD4$^+$ T cells capable to re-express and reassembles CENP-A upon cell cycle entry, demonstrating the physiological importance of the genetic memory.

Keywords CENP-A; CENP-B; centromere; chromatin; chromosome segregation

Subject Categories Cell Cycle; Chromatin, Transcription & Genomics

DOI 10.15252/embj.2020105505 | Received 3 May 2020 | Revised 10 August 2020 | Accepted 25 August 2020

The EMBO Journal (2020) e105505

Introduction

Proper transmission of genetic information at each cell division is vital to healthy development and survival. Centromeres are key in maintaining a correct karyotype. In monocentric species, abnormalities in their number or integrity lead to mitotic defects (Barra & Fachinetti, 2018). Thus, cells must preserve a unique centromere per chromosome to prevent the emergence of genomic instability. In most species including humans, this is achieved via a robust epigenetic self-assembly loop that ensures the replenishment of centromeric proteins at the same location for an indefinite number of cell cycles (McKinley & Cheeseman, 2016).

The most striking evidence that centromere position is epigenetically identified derives from the discovery of stably inherited neocentromeres in human patients (Voullaire *et al*, 1993). In these cases, a centromere has been formed on an ectopic position along the chromosome arm at non-centromeric DNA sequences. Except rare cases, human neocentromeres are associated with chromosomal rearrangements, entailing the partial or total excision of the original centromeric DNA (CenDNA), and are found in developmental diseases and some types of tumors (Marshall *et al*, 2008).

In the last two decades, many reports have converged toward the evidence that in most species, the CENtromere Protein A (CENP-A), a specialized histone H3 variant enriched at centromeric regions (Earnshaw & Rothfield, 1985; Palmer *et al*, 1987), is the centromeric epigenetic mark (Fukagawa & Earnshaw, 2014). Through a tight regulatory process (Zasadzińska & Foltz, 2017), CENP-A maintains centromere position via a two-step mechanism (Fachinetti *et al*, 2013). First, at mitotic exit CENP-A self-directs its assembly (template model) to maintain its centromere localization (Jansen *et al*, 2007) via the CENP-A Targeting Domain (CATD) (Black *et al*, 2004, 2007; Foltz *et al*, 2009; Bassett *et al*, 2012), at which new CENP-A molecules are assembled adjacent to the existing ones (Ross *et al*, 2016). Subsequently, CENP-A promotes the assembly of several centromeric components, collectively named the Constitutive Centromere-Associated Network (CCAN) complex (Foltz *et al*, 2006; Hori *et al*, 2008; Weir *et al*, 2016; Pesenti *et al*, 2018), mostly via a direct interaction with CENP-C and CENP-N (Carroll *et al*, 2009, 2010; Guse *et al*, 2011; Kato *et al*, 2013). In turn, the CCAN complex is required to assemble the kinetochore (Musacchio & Desai, 2017).

In vertebrates, CENP-A incorporation into chromatin is mediated by a specific chaperone, HJURP (Dunleavy *et al*, 2009; Foltz *et al*, 2009; Bernad *et al*, 2011) that forms a complex with acetylated histone H4 (Sullivan & Karpen, 2004; Bailey *et al*, 2016; Shang *et al*, 2016). The HJURP/CENP-A/H4 complex is directed to the

1 Institut Curie, CNRS, UMR 144, PSL Research University, Paris, France
2 Institut Curie, PSL Research University, INSERM U932, Paris, France
3 Department of Molecular Genetics and Microbiology, Duke University Medical Center, Durham, NC, USA
*Corresponding author. Tel: +33 1 56246335; E-mail: daniele.fachinetti@curie.fr
†These authors contributed equally to this work

centromere via the Mis18 complex (Barnhart *et al*, 2011; Wang *et al*, 2014; Nardi *et al*, 2016; Pan *et al*, 2019), an octameric protein complex (M18BP1 and Mis18α/β subunit) that licenses new CENP-A deposition (Moree *et al*, 2011; Dambacher *et al*, 2012). How the Mis18 complex recognizes centromeres is still a matter of investigation, but M18BP1 and Mis18β were shown to interact with the C-terminal domain of CENP-C (Moree *et al*, 2011; Dambacher *et al*, 2012; Stellfox *et al*, 2016; Pan *et al*, 2017) or directly with CENP-A in both chicken (Hori *et al*, 2017) and frogs (French *et al*, 2017) (although the residue involved in this interaction is missing in humans). Polo-like kinase 1 (PLK-1) and cyclin-dependent kinases (CDK) 1 and 2 ensure the cell cycle regulation of both HJURP and Mis18 complex (Silva *et al*, 2012; McKinley & Cheeseman, 2014; Müller *et al*, 2014; Stankovic *et al*, 2016; Pan *et al*, 2017).

Despite the strong indication that the self-assembly loop mediated by CENP-A uniquely defines centromere position, native human centromeres are always associated with long stretches of repetitive tandemly arranged DNA sequences named alpha satellites (Allshire & Karpen, 2008). Intriguingly, in mammals, fission yeast, and insects, these tandem repeats acquired, over evolution, a DNA sequence-specific binding protein (CENP-B or CENP-B-related proteins) (Gamba & Fachinetti, 2020). In humans, CENP-B binds to a specific motif named CENP-B box that is present within the alpha-satellite unit at all centromeres, except the Y chromosome (Earnshaw *et al*, 1989; Miga *et al*, 2014). Why centromeres are built over tandem repeats and why CENP-B evolved to bind CenDNA, although it is not present in all organisms, are still open questions.

The role of CENP-B and repetitive DNA at centromeres has puzzled researchers for years. On the one hand, CENP-B appears to be non-essential since it is absent from the Y centromere (Earnshaw *et al*, 1989) and from stably inherited neocentromeres (Voullaire *et al*, 1993), and CENP-B knock-out mice are viable (Hudson *et al*, 1998; Kapoor *et al*, 1998; Perez-Castro *et al*, 1998). Conversely, we showed that CENP-B bound to CenDNA is important to maintain chromosome segregation fidelity (Fachinetti *et al*, 2015; Hoffmann *et al*, 2016) by counteracting chromosome-specific aneuploidy during mitosis (Dumont *et al*, 2020). Beside their active role in chromosome segregation, CenDNA and CENP-B were also implicated in favoring the establishment of functional human artificial chromosomes (HACs) (Ohzeki *et al*, 2002; Okada *et al*, 2007), possibly by recruiting CENP-A directly via the CENP-B amino-terminal tail (Fujita *et al*, 2015). However, recently, *Logsdon et al* described that HAC formation is not strictly dependent on alpha-satellite sequences or CENP-B (Logsdon *et al*, 2019). Interestingly, in half of the cases of α-satellite-free HAC formation, centromeric DNA was acquired within their sequence, somewhat supporting a role for CenDNA during mini-chromosome formation.

Hence, whether CENP-B and the underlying CenDNA are required for *de novo* centromere formation of naturally occurring human centromeres and/or if they contribute to centromere identity remains elusive.

Here, we explore the importance of repetitive DNA sequences in centromere specification at native human centromeres by generating an inducible depletion and re-activation system of the centromeric epigenetic mark CENP-A. With this unique approach, we reveal the order of events necessary to maintain centromere position in human cells. We uncover the importance of CENP-B binding to CenDNA in centromere specification at native human centromeres by preserving a critical level of CENP-C necessary to promote *de novo* CENP-A assembly. Our work has both physiological and pathological implications as demonstrated by the existence of CENP-A-negative resting $CD4^+$ T lymphocytes capable to re-enter in the cell cycle and the formation of neocentromeres in a CENP-B-negative chromosome, respectively.

Results

Previously deposited CENP-A is not essential for new CENP-A deposition at endogenous centromeres

CENP-A is well known to maintain centromere position via an epigenetic self-assembly loop (McKinley & Cheeseman, 2016). This suggests that at least a pool of CENP-A must always be maintained at the centromere to mediate new CENP-A deposition. Here, we sought to challenge this concept and test if previously deposited centromeric CENP-A is required to license new CENP-A deposition at the native centromere position. To this aim, we used a two-step assay (hereafter referred to as $CENP\text{-}A^{OFF/ON}$ system) that allows us, in a first step, to deplete endogenous CENP-A and, subsequently, to re-express it (Fig 1A). To generate this unique tool/model, we took advantage of the reversibility of the auxin-inducible degron (AID) system that allows rapid protein depletion and re-accumulation following synthetic auxin (indol-3-acetic acid, IAA) treatment and wash-out (WO), respectively (Nishimura *et al*, 2009; Holland *et al*, 2012; Hoffmann & Fachinetti, 2018). By combining genome editing

Figure 1. The CENP-A epigenetic self-assembly mechanism is not required for *de novo* CENP-A deposition at native human centromere.

A Schematic illustration of the two-step $CENP\text{-}A^{OFF/ON}$ assay using the auxin (IAA) inducible degradation system.

B Immunoblot showing $CENP\text{-}A^{EA}$ protein level at the indicated time in RPE-1 cells.

C Representative immunofluorescence images showing CENP-A reloading at CENP-B-marked centromeres. White dashed circles contour nuclei. Scale bar, 5 μm.

D Quantification of the percentage of cells showing centromeric CENP-A 24 or 48 h after IAA WO. Each dot represents one experiment (~30–50 cells per condition per experiment), and error bars represent standard deviation (SD) of 5 independent experiments.

E Quantification of centromeric CENP-A levels normalized to non-treated level. Each dot represents one experiment, and error bars represent SD. Unpaired *t*-test: $***P = 0.0005$.

F Stills of live cell imaging to follow *de novo* $CENP\text{-}A^{EA}$ reloading in RPE-1 cells harboring endogenously tagged $CENP\text{-}B^{mcherry}$. Images were taken every 15 min. White dashed circles contour nuclei prior/after mitosis and cells during mitosis based on bright-field images. Scale bar, 10 μm.

G Dot plot showing the timing of $CENP\text{-}A^{EA}$ reloading after anaphase onset in the indicated cell lines. Each dot represents one cell, and error bars represent standard deviation. Unpaired *t*-test, ns.

Source data are available online for this figure.

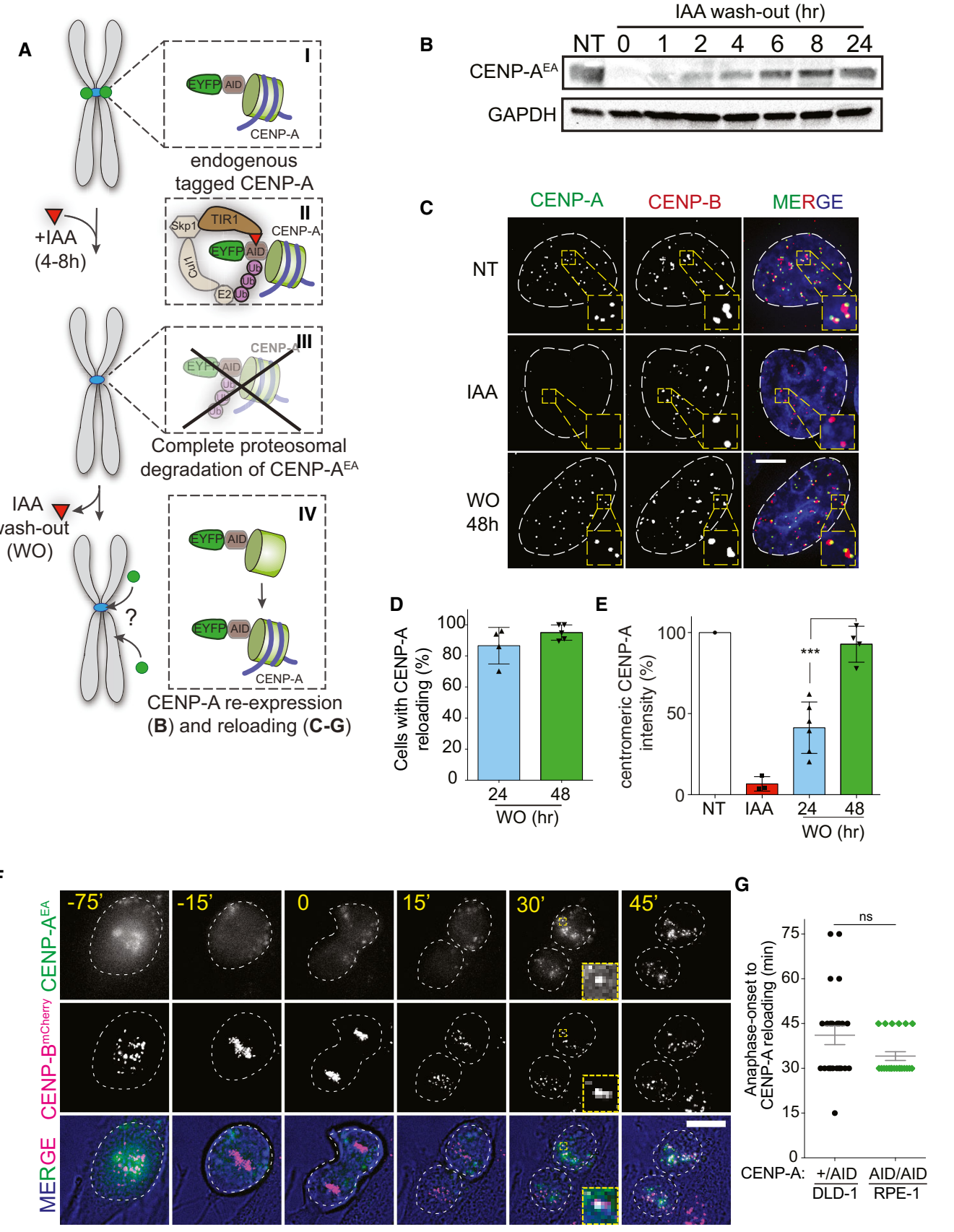

Figure 1.

with the AID tagging system, we previously showed our ability to rapidly and completely remove endogenous CENP-A from human centromeres with a half-life of about 15 min (Hoffmann *et al*, 2016), with only a small percentage of cells that remain unaffected by the IAA treatment (Fig EV1A). Following IAA WO, endogenous CENP-A$^{EYFP\text{-}AID}$ (hereafter referred to as CENP-A^{EA}) is rapidly (within 1–2 h) re-expressed at detectable level as observed by immunoblot (Fig 1B). The rapid CENP-A re-accumulation could be explained by the continuous presence of mRNA CENP-A transcripts despite the immediate protein degradation in the presence of IAA. Hence, the generated CENP-A$^{OFF/ON}$ system provides a powerful tool to test CENP-A reloading in the absence of previously deposited CENP-A.

We next tested if newly expressed CENP-A is reloaded back at the native centromere position by immunofluorescence (IF). Following CENP-A depletion for 4–8 h and IAA WO for 24 or 48 h, we found that in most (~90%) of the cells, newly expressed CENP-A relocalizes with centromeric regions marked by CENP-B, which remains tightly bound to the CENP-B boxes (Fig 1C–E). Interestingly, centromeric CENP-A levels recovered to only ~50% of untreated levels after one cell cycle (24-h WO), but fully recovered to untreated levels after IAA 48-h WO (Fig 1E). This was due to incomplete recovery of total CENP-A levels rather than the absence of preexisting CENP-A molecules or preexisting centromeric factors that mediate CENP-A assembly. Indeed, centromeric CENP-A amount recovered to untreated levels within one cell cycle when we prolonged G2 phase—time where most CENP-A is transcribed (Shelby *et al*, 1997)—after IAA WO using a CDK1 analog sensitive inhibition system (Hochegger *et al*, 2007; Saldivar *et al*, 2018) (Fig EV1B and C). Following short-term CENP-A depletion, many CCAN components partially remain at centromeric regions (Hoffmann *et al*, 2016), potentially promoting CENP-A deposition (Okada *et al*, 2006; Hori *et al*, 2008; McKinley *et al*, 2015). We thus depleted CENP-A for longer durations (24–48 h) as, in these conditions, most CCAN proteins are lost from centromeres (Hoffmann *et al*, 2016). We used p53-deficient DLD-1 cells and chromosomally unstable U-2OS cells to bypass cell cycle block due to events of chromosome mis-segregation following CENP-A depletion. Even in these conditions, newly expressed CENP-A molecules were reloaded at CENP-A-depleted centromeres (Fig EV1D).

We then followed *de novo* CENP-A reloading using live cell imaging taking advantage of the EYFP tag on the endogenous CENP-A (Hoffmann *et al*, 2016). To mark centromere position in live cells, we endogenously tagged CENP-B with mCherry using CRISPR/Cas9 in RPE-1 cells. Following the induction of a CENP-A$^{OFF/ON}$ cycle, we observed a burst of reloading of CENP-A shortly after mitotic exit (approximately 30 min after anaphase onset) (Fig 1F and G, Movie EV1), in agreement with the previously described timing of CENP-A reloading (Jansen *et al*, 2007). This experiment showed that CENP-A reloading in the absence of any previously deposited centromeric CENP-A is still tightly restricted to a narrow cell cycle window. So, we further examined if *de novo* CENP-A reloading relies on the same key regulation mechanisms as canonical CENP-A deposition (McKinley & Cheeseman, 2016). We confirmed that *de novo* CENP-A deposition is dependent on M18BP1 and HJURP, but not DAXX, a histone chaperone that was shown to be involved in non-centromeric CENP-A deposition (Lacoste *et al*, 2014) (Fig EV1E–K). However, as HJURP depletion strongly impacts the stability of soluble CENP-A, re-expression of CENP-A was also strongly affected by HJURP depletion making a direct conclusion on HJURP dependency uncertain (Fig EV1K).

Altogether, our data indicate that centromere position is preserved even in the absence of CENP-A. Also, it demonstrates that previously assembled CENP-A is not essential for *de novo* deposition of CENP-A nor to control its abundance, as levels of new CENP-A rise very fast at CENP-A-depleted centromeres, a result in disagreement with the template model. Further, like canonical CENP-A reloading in the presence of previously deposited CENP-A, *de novo* CENP-A reloading is cell cycle regulated and occurred exclusively after mitotic exit.

Our results rely on complete depletion of CENP-A following IAA addition, as we have previously shown by IF, immunoblot and immunoprecipitation (Hoffmann *et al*, 2016). To further prove the efficiency of the auxin system, we challenged it by inducible, doxycycline-mediated overexpression (OE) of CENP-A tagged with EYFP and AID (Fig EV2A). CENP-A OE leads to elevated CENP-A incorporation at the centromere and also outside the centromere region (Lacoste *et al*, 2014; Nechemia-Arbely *et al*, 2017). Using this system, we obtained ~2,000-fold higher nuclear CENP-A^{EA} protein level as compared to endogenous CENP-A levels at a single centromere (Fig EV2B and C). Despite the vast excess of CENP-A in these cells, no CENP-A was detectable upon IAA addition by IF (Fig EV2B and C). We concluded that the AID system remains—by far—unsaturated under endogenous CENP-A expression level conditions, as we are able to deplete higher CENP-A^{EA} levels to non-detectable level.

We then used live cell single molecule microscopy (SMM) to assess the presence of single CENP-A molecules tagged with EYFP after IAA addition. We first confirmed the ability to detect a single EYFP molecule by transiently expressing EYFP-tagged Glucocorticoid Receptor (GR^{EYFP}) as it was previously used to study dynamics of single molecules in human cells (Harkes *et al*, 2015) (Fig EV2D). Here, we observed a clear diffraction limited spot with a Gaussian profile that bleached in a single bleach step as expected when observing a single molecule (Fig EV2E–G). In contrast, we were unable to detect such profile for CENP-A^{EA} at CENP-B^{mCherry}-positive centromeres following IAA treatment. Quantification of EYFP fluorescent intensities of IAA-treated CENP-A^{EA} cells at centromeres was significantly lower than the fluorescent signal of a GR^{EYFP} single molecule and comparable to the background signal obtained in EYFP-free RPE-1 CENP-C$^{mCherry\text{-}AID}$ cells (Fig EV2E–G).

In summary, we concluded that CENP-A reloading following CENP-A$^{OFF/ON}$ is unlikely to be due to any remaining CENP-A molecules. In addition, as CENP-A loading occurs only at mitotic exit, the dynamic equilibrium between its IAA-mediated degradation and re-expression does not influence our results.

De novo CENP-A localization remains unaltered in the absence of old centromeric CENP-A

Human centromeres display a hierarchical organization ultimately structured as higher order repeat arrays (HOR) (Miga, 2017). Some chromosomes have centromeres with multiple HOR arrays which display different abundance of CENP-B boxes and CENP-A occupancy (Sullivan *et al*, 2011). In some cases (e.g., chromosomes 7 or 17), the two homologue chromosomes display equal CENP-A

occupancy but at different HOR arrays (epiallelic status) (Maloney *et al*, 2012). Also, it has been demonstrated that inactive HOR arrays with low CENP-A occupancy have the capacity to trigger HAC formation (Maloney *et al*, 2012). The CENP-A self-assembly mechanism model implies that previously incorporated CENP-A is required to avoid the sliding of the centromere to a different chromosomal position.

Using the CENP-A$^{OFF/ON}$ system, we tested if *de novo* CENP-A deposition was slightly displaced ultimately leading to a different distribution at HOR arrays within the same centromeric locus (Fig 2A). CENP-A—HOR array occupancy was determined by CUT&RUN (Cleavage Under Targets and Release Using Nuclease) combined with high-throughput sequencing (Skene & Henikoff, 2017). Sequencing reads were mapped to the latest HOR reference assembly for centromeric sequences, as described previously (Dumont *et al*, 2020). In agreement with previous observations of CENP-A occupancy, in untreated cells, CENP-A localized mostly to a defined HOR, but it could also be found on different HORs of the same chromosome (Sullivan *et al*, 2011; Nechemia-Arbely *et al*, 2019). Following CENP-A depletion and re-activation, we found that the distribution of *de novo* CENP-A along the different HORs was maintained, as we did not observe any remarkable differences in CENP-A HOR array occupancy compared to the untreated condition (Figs 2B–D and EV2H). These results were confirmed by line scan and by chromatin fiber techniques coupled with FISH (Fig EV2I and J). Here, we determined CENP-A occupancy along the HOR array of chromosome X (DXZ1) and found that CENP-A re-occupies around 35% of the DXZ1 array within 48 h (Fig EV2I), similar to the control and in agreement with previous results (Maloney *et al*, 2012).

Altogether, we concluded that CENP-A is reloaded at the same HOR array even in the absence of previously deposited CENP-A and that (epi-)genetic mechanism(s) other than CENP-A are involved in maintaining centromere position.

To further test the importance of the original centromere location, we then generated an *in vivo* competition assay between the native centromeres lacking endogenous CENP-A and ectopic site(s) enriched with exogenous CENP-A. To do so, we used an inducible CENP-A OE system with a binary (on/off) controllable activity in the CENP-A$^{OFF/ON}$ background. This binary control is achieved via a doxycycline-inducible expression of CENP-A tagged with a destabilization domain *E. coli*-derived DiHydroFolate Reductase (DHFR) protein (Fig 2E). Addition of a small ligand named TriMethoPrim (TMP) is required for protein stabilization (Iwamoto *et al*, 2010). We then assessed if *de novo* endogenous CENP-A reloads at non-centromeric sites following mis-incorporation of exogenous CENP-A—which can be indistinguishable from centromeric CENP-A (Fig 2F)—and if this was sufficient to trigger ectopic centromere formation (Fig 2G). In most analyzed cases, centromere function (defined by the presence of CENP-C) was occurring at CENP-B marked centromeres and never observed at ectopic loci despite the initial presence of ectopic CENP-A along the chromosome arms (Fig 2H and I).

These data demonstrate the importance of alpha-satellite DNAs and their embedded features in marking centromere position.

De novo CENP-A deposition is impaired in CENP-B-deficient cells

We next asked what maintains centromere position in the absence of previously deposited CENP-A. We have already demonstrated that CENP-B plays a major role in stabilizing centromere proteins, including a fraction of CENP-C, on CENP-A-depleted centromeres (Hoffmann *et al*, 2016). We therefore hypothesized that CENP-B may be important for *de novo* CENP-A deposition. To test this, we assessed CENP-A *de novo* deposition in *CENP-B* KO RPE-1 cells harboring the CENP-A$^{OFF/ON}$ system (Hoffmann *et al*, 2016). Following CENP-A$^{OFF/ON}$, we found that *de novo* CENP-A reloading was strongly impaired in *CENP-B*$^{-/-}$ cells compared to *CENP-B*$^{+/+}$ cells, with < 20% of the cells that reloaded CENP-A upon re-expression (Fig 3A–C).

Co-depletion of CENP-A and CENP-B leads to immediate mitotic defects (Hoffmann *et al*, 2016) that result in a p53-mediated cell cycle arrest. So, we first tested if massive chromosome mis-segregation *per se* has an effect on *de novo* CENP-A reloading by chemical inhibition of the spindle checkpoint kinase Mps1 (Santaguida & Musacchio, 2009). Despite massive chromosome mis-segregation in this condition, *de novo* CENP-A reloading was not affected (Fig EV3A–C). To rule out that failure of *de novo* CENP-A deposition in *CENP-B* KO cells is not simply a consequence of cell cycle arrest, we depleted *CENP-B* using CRISPR in a p53-deficient DLD-1 cell line (Fig EV3D). We then synchronized cells to specifically assess *de novo* CENP-A reloading uniquely in cells that underwent mitosis following the CENP-A$^{OFF/ON}$ pulse (Fig 3D). Using α-tubulin staining to visualize early G1 cells, we found that ~90% of *CENP-B*$^{-/-}$ cells showed impaired *de novo* CENP-A reloading while almost all *CENP-B*$^{+/+}$ cells successfully reloaded CENP-A (Fig 3E and F), similar to control RPE-1 cells. Interestingly, ~50% of the *CENP-B*$^{-/-}$ cells failed to reload CENP-A completely, while around 40% of cells showed only partial reloading of CENP-A with less than 10 centromeric CENP-A dots per daughter cell (Figs 3E and F, and EV3E). We then tested if re-expression of CENP-B could rescue CENP-A *de novo* deposition in CENP-B KO cells. To this aim, we integrated CENP-B into an isogenic FRT locus that can be induced by doxycycline addition. Following a CENP-A$^{OFF/ON}$ pulse, most cells rescued by CENP-B successfully reloaded CENP-A to a similar extent as the CENP-B wild-type cell line (Fig EV3F and G).

Overall, our data demonstrate that CENP-B is required for efficient reloading of *de novo* CENP-A in the absence of any previously deposited centromeric CENP-A

Neocentromere formation occurs on the Y chromosome under selective pressure

The centromere of the Y chromosome contains repetitive alpha-satellite DNA sequences but lacks CENP-B binding sites. Hence, CENP-B is absent from the Y centromere (Earnshaw *et al*, 1989; Miga *et al*, 2014). To assess *de novo* CENP-A reloading at the Y centromere, we used Fluorescence *In Situ* Hybridization (FISH) probes against the Y centromere or the X centromere, as a control, in combination with IF in interphase cells and on metaphase spreads in DLD-1 cells (Fig 4A and B). Following a CENP-A$^{OFF/ON}$ cycle, *de novo* CENP-A or CENP-C colocalized with the X centromere in both interphase and metaphase spreads, respectively, with no significant changes in abundance when compared to non-treated cells or to single allele AID-tagged CENP-A$^{AID/+}$ cells (Fig 4C and D and Appendix Fig S1A and B). Conversely, only ~25% of cells showed CENP-A/CENP-C at the Y centromere in both interphase (Appendix Fig S1A and B) and mitotic (Fig 4C and D) cells. So, as

observed in *CENP-B* KO cells, *de novo* CENP-A reloading is impaired at CENP-B lacking centromeres.

We then studied whether CENP-A deposition can occur at a different, non-alpha-satellite location after CENP-A re-expression. However, the Y chromosome is not an essential chromosome in the *in vitro* cell culture model, and since neocentromere formation happens at very low frequency (Shang *et al*, 2013), the impaired CENP-A reloading is expected to lead to the loss of the Y chromosome in the majority of cells (Ly *et al*, 2017). To prevent its loss, we selected for the retention of the Y chromosome by inserting a selectable cassette (neomycin) (Fig 4E and Appendix Fig S1C and D). Following CENP-A depletion and re-activation, we subjected cells to G418 treatment to select clones that maintained the Y chromosome (neomycin positive), as observed by colony formation assay (Appendix Fig S1E). Following a CENP-A$^{OFF/ON}$ cycle, we observed a strong impact of G418

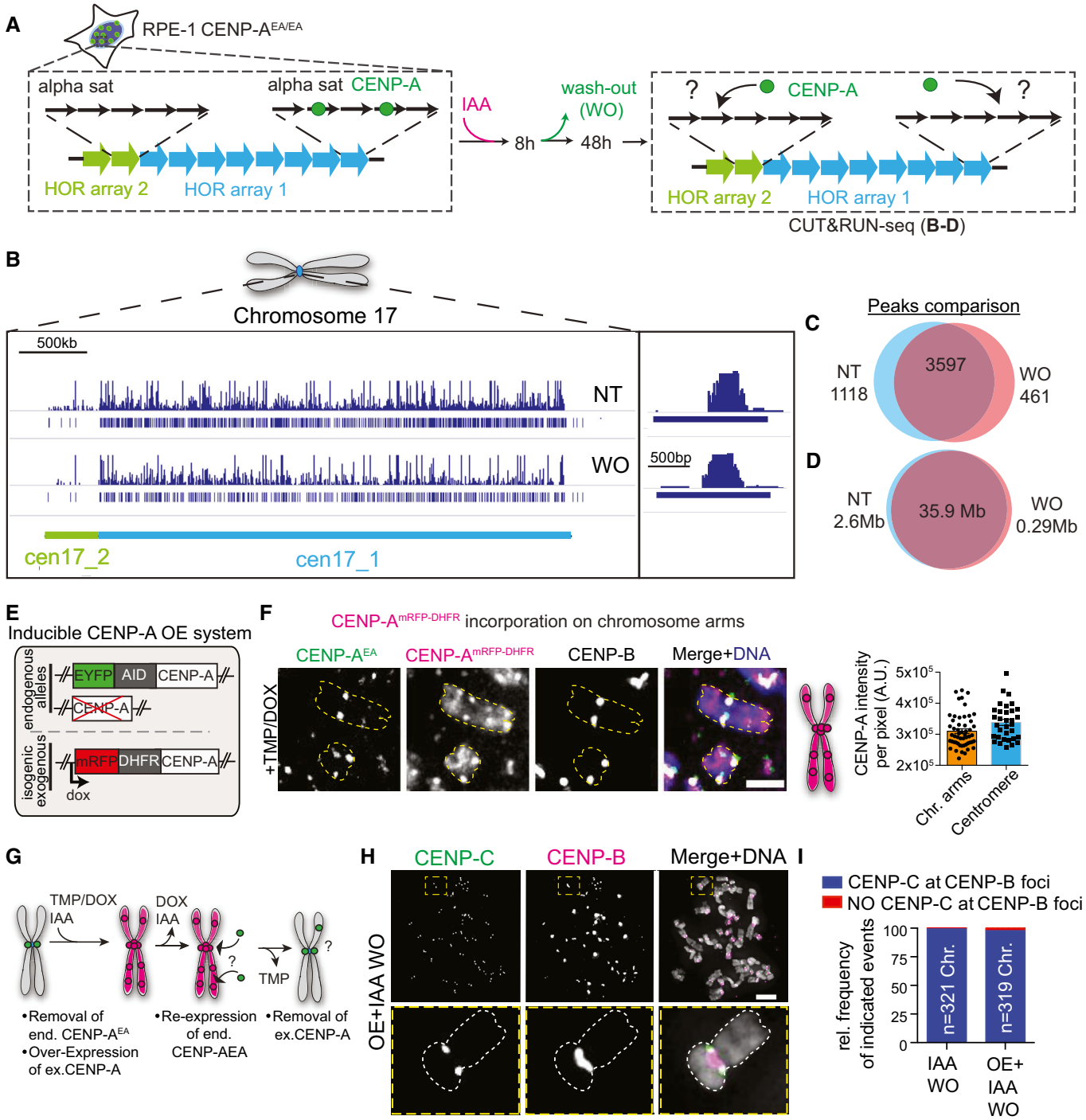

Figure 2.

Figure 2. Previously deposited CENP-A is dispensable for precise *de novo* CENP-A incorporation.

A Schematic of DNA sequence organization at centromeres with more than one higher order repeat array (HOR) and experimental set-up of the CENP-A$^{OFF/ON}$ cycle performed in experiments B-D.

B Full coverage plot of chromosome 17 centromeric array (chr17:22,500,000–26,900,000 of the hg38 assembly) showing enrichment of CENP-A by CUT&RUN-seq in the untreated (NT) and IAA wash-out (WO) sample. CENP-A is reloaded to cen17_1 (D17Z1). A shift of CENP-A occupancy to cen17_2 (D17Z1B) is not detected.

C Venn diagram showing the number of CUT&RUN-seq peaks that are NT specific (left, blue), WO specific (right, red), or overlapping (center).

D Venn diagram showing the total length in Mb of CUT&RUN-seq peaks that are NT specific (left, blue), WO specific (right, red), or shared between NT and WO (center).

E Illustration of genomic make-up of DLD-1 with an exogenous CENP-A$^{mRFP\text{-}DHFR}$ overexpression system.

F Representative images showing ectopic CENP-A on a chromosome spread after induction of CENP-A overexpression in DLD-1 cells. Centromere position is marked using immunofluorescence staining for CENP-B. Yellow dashed lines contour representative chromosomes. Scale bar, 2 μm. Schematic to the right illustrates the observed CENP-A$^{mRFP\text{-}DHFR}$ localization pattern on a chromosome. Right panel: Comparison of CENP-A^{DHFR} level per pixel at the centromere and on chromosome arms following IAA and DOX/TMP treatment. Each dot represents one centromere or a region on the chromosome arms.

G Schematic illustration for the experiments shown in H, I.

H Representative images of chromosome spreads after re-expression of endogenous CENP-A^{EA} into a CENP-A$^{mRFP\text{-}DHFR}$ overexpression background and subsequent removal of the overexpression as illustrated in (G). Antibody against CENP-C was used to score for the presence of the functional centromere. Scale bar, 5 μm.

I Quantification of the indicated events after one CENP-A$^{OFF/ON}$ cycle compared to treatment shown in (G).

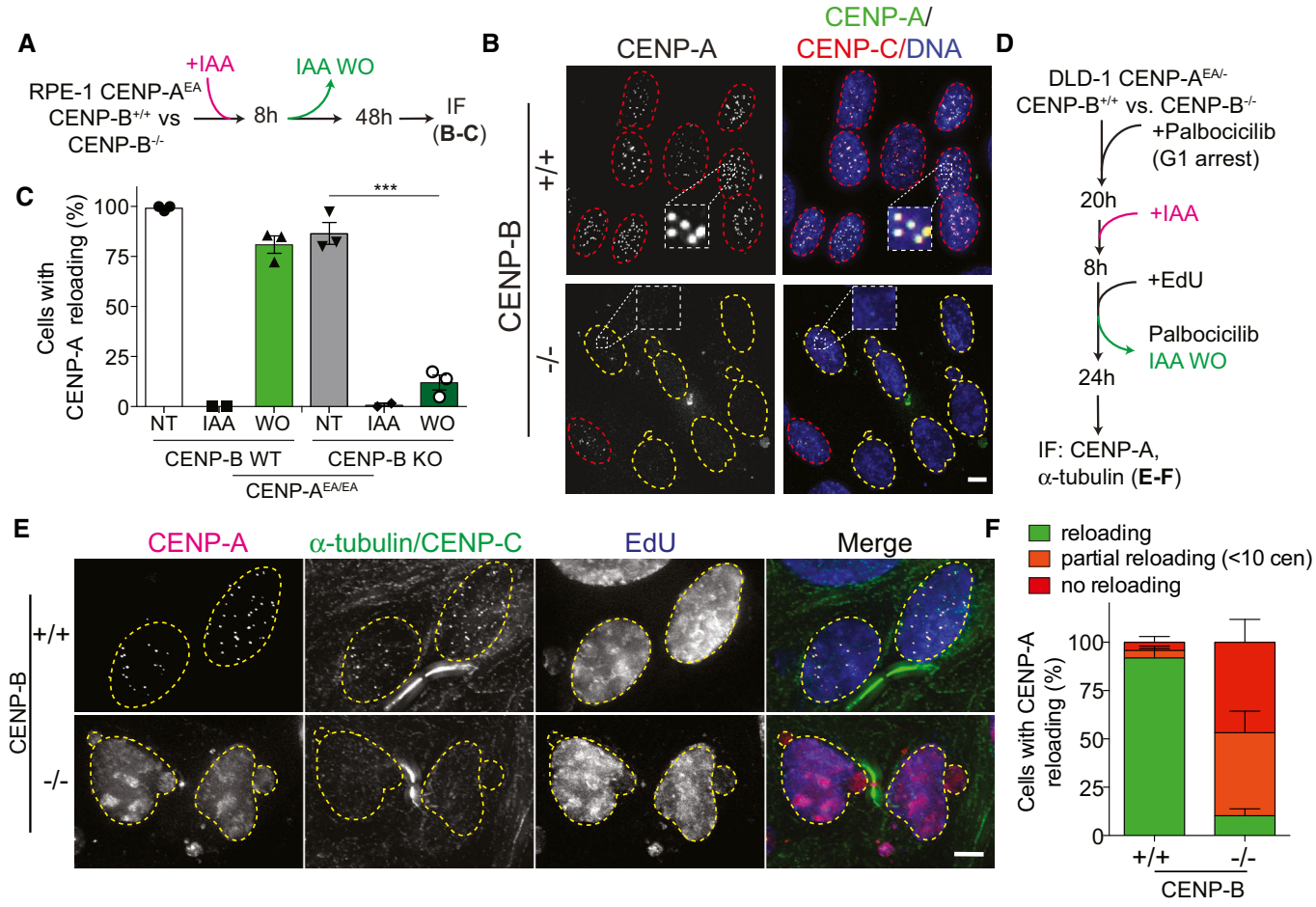

Figure 3. *De novo* CENP-A deposition is impaired in the absence of CENP-B.

A Schematic illustration of the CENP-A$^{OFF/ON}$ cycle performed in the experiments shown in B, C.

B Representative images of *de novo* CENP-A reloading in *CENP-B* wild-type (+/+) and *CENP-B* knock-out (−/−) cells. Cells with centromeric CENP-A are marked with a red dashed contour line, while a yellow contour lines mark cell without centromeric CENP-A. Scale bar, 5 μm.

C Quantification of relative number of RPE-1 cells with centromeric CENP-A in the indicated conditions. Each dot represents one experiment with at least 20 cells per condition. Error bars represent standard error of the mean (SEM) from 3 independent experiments. Unpaired *t*-test, ***P = 0.0003.

D Schematic representation of experiments shown in E, F.

E Representative images of DLD-1 CENP-B (+/+) or (−/−) cells in late M phase following one CENP-A$^{OFF/ON}$ cycle. EdU staining was used to confirm successful wash-out of palbociclib and cell progressing through S-phase. Yellow dashed lines contour nucleus of cells in late M phase. Scale bar 5 μm.

F Quantification of indicated events observed in late M phase cells in the indicated cell lines. Error bars show SEM from 4 independent experiments.

selection on cell viability that likely reflects failure of CENP-A deposition on the Y chromosome and subsequent loss of the chromosome bearing the selection marker. IF-FISH on the pool of surviving clones revealed three outcomes: (i) In ~70% of the cells, CENP-C was found to be at the original Y centromere location, indicating that other centromere features different from CENP-A and CENP-B favor centromere formation at native centromere position (Fig 4F–H); (ii) in about 15% of the cells, the entire or portions of the Y chromosome (likely containing the neomycin cassette) was fused to other chromosomes, an event that could be observed also in untreated condition, although at very low frequency (Fig 4G and H); (iii) intriguingly, in the about 15% of remaining cases, CENP-C staining was observed elsewhere on the Y chromosome, and not coinciding with the Y centromeric probe, indicating the presence of a neocentromere (Fig 4G and H). Importantly, neocentromere-like elements were exclusively

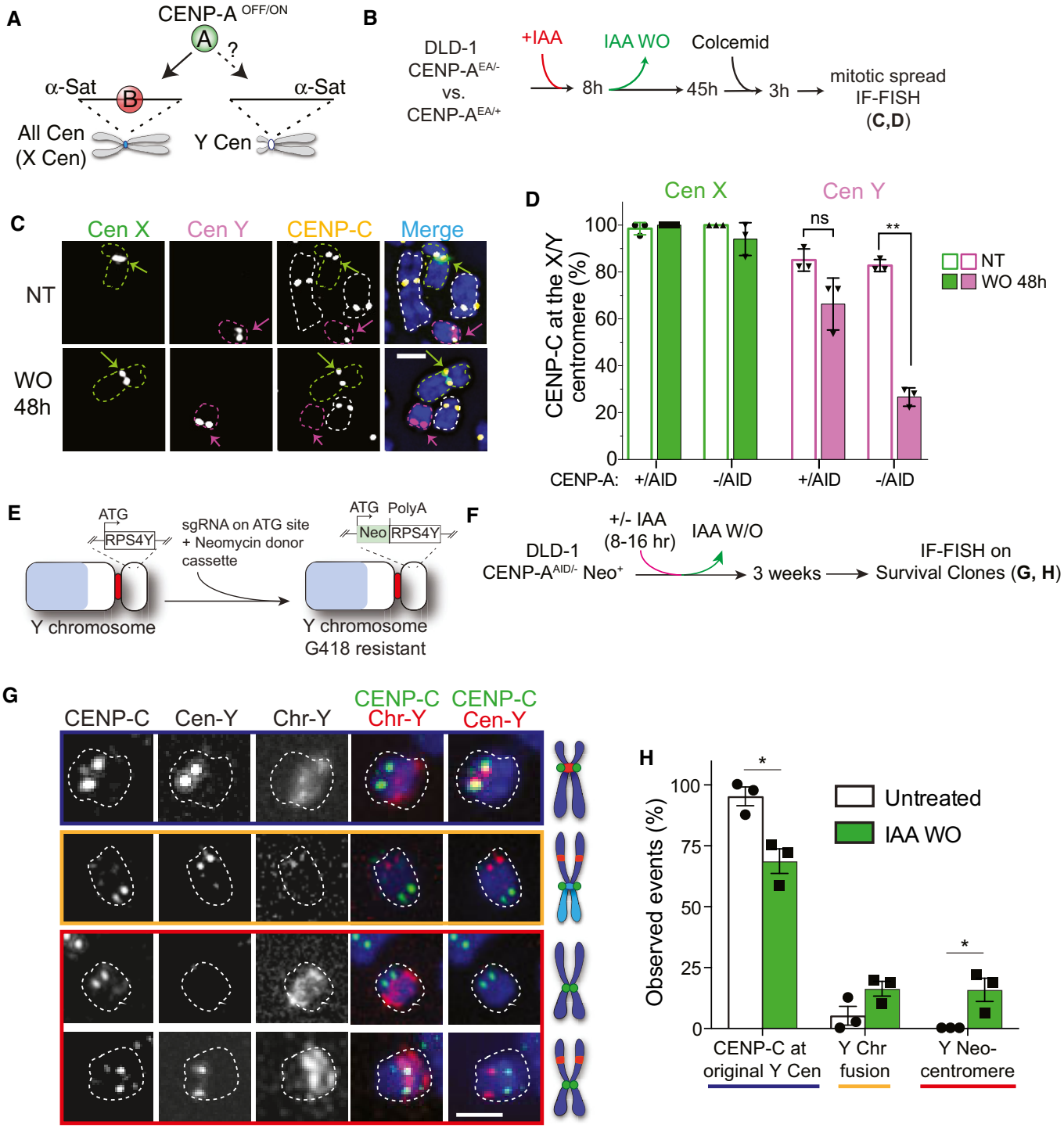

Figure 4.

Figure 4. Neocentromere formation arises at the CENP-B-negative Y chromosome.

A Concept of experiments shown in B-D.

B Timeline of experiment performed in C, D.

C Representative IF-FISH images of mitotic spreads in non-treated cell (NT) and following a CENP-A$^{OFF/ON}$ cycle (IAA WO). Chromosomes are contoured by a green (X), magenta (Y), or white (other autosomes) dashed line. The centromeres of chromosome X/Y are highlighted by a green/magenta arrow. Scale bar, 2 μm.

D Quantification of CENP-C (as read-out of CENP-A) presence at the X (green) or Y (magenta) centromere in the indicated cell lines. Each dot represents one experiment. Error bars represent SD from 3 independent experiments. Unpaired *t*-test, $^{**}P = 0.0042$.

E Schematic illustration of CRISPR/Cas9-mediated genome editing of the non-essential RPS4Y gene on the Y chromosome with the insertion of a neomycin resistance cassette.

F Experimental set-up for G, H.

G Representative IF-FISH images showing CENP-C localization on the Y chromosome in cell growing under selective pressure (G418) following a CENP-A$^{OFF/ON}$ cycle. Chromosomes are highlighted by a white dashed contour line. CENP-C was found at the native centromere position (top panel, blue), the Y chromosome fused to another chromosome indicated by the increased size of the chromosome and the absence of Chr-Y painting probe staining (second panel, orange) or CENP-C was found on a different location on the Y chromosome and did not overlap with Cen-Y DNA (lower panels, red). Scale bar, 2 μm.

H Quantification of indicated events depicted in G. Each dot represents one experiment (> 20 spreads for experiment). Error bars represent SEM from 3 independent experiments. Unpaired *t*-test, $^{*}P = 0.0137$ and 0.039.

found after CENP-A depletion and re-activation by IAA WO, but never under untreated conditions (Fig 4H).

These data indicate that neocentromere-like elements can form on a CENP-B-deficient chromosome following rapid CENP-A re-expression, but only when CENP-A-mediated centromere identity was transiently perturbed. Nevertheless, native centromere location continues to be the preferential site for centromere re-formation.

CENP-B bound to an ectopic location promotes CENP-C recruitment independently of CENP-A

We next investigated how CENP-B maintains centromere position at native centromeres. Previous studies showed that CENP-C interacts with CENP-B directly (Suzuki *et al*, 2004; Fachinetti *et al*, 2015), in addition to its well-known interaction with CENP-A (Guse *et al*, 2011; Fachinetti *et al*, 2013; Kato *et al*, 2013). Here, we noticed that exogenous CENP-B expression not only rescued *de novo* CENP-A reloading in CENP-B$^{-/-}$ cells (Fig EV3G), but also lead to increased CENP-C levels at the centromeres that were mostly maintained even after CENP-A depletion (Appendix Fig S2A and B). These observations indicate that CENP-B not only maintains and stabilizes CENP-C (Hoffmann *et al*, 2016), but might also recruit CENP-C *de novo* to the centromere.

To test this hypothesis, we used the LacO-LacI system in a previously described U-2OS cell line (Janicki *et al*, 2004) in which we further integrated the CENP-A$^{OFF/ON}$ system at the CENP-A endogenous locus. This system allows us to test whether CENP-B can recruit CENP-C to an ectopic LacO locus independently of CENP-A (Fig 5A). Following transfection of CENP-B-LacI-mCherry, CENP-C recruitment to the ectopic big LacI/CENP-B sites was observed in the majority of the cells, even upon IAA treatment to deplete CENP-A, in contrast to the LacI/mCherry control (Fig 5B–D). Interestingly, CENP-C molecules at the LacO array were organized in patches rather than covering LacO sites homogenously. Based on previous studies (Hori *et al*, 2013; Shono *et al*, 2015), we predicted that once CENP-C is recruited to the LacO array, it should recruit CENP-A. Indeed, following IAA WO, CENP-A was recruited at most CENP-B/CENP-C-positive LacO arrays (Fig 5C–E). Efficient recruitment of CENP-A was dependent on CENP-C, as pre-removal of CENP-C by siRNA largely abolished CENP-A recruitment at CENP-B-positive LacO arrays (Appendix Fig S2C–G). Residual CENP-A recruitment in this condition could be due to incomplete CENP-C depletion by siRNA or to a weak ability of CENP-B to directly recruit CENP-A (Fujita *et al*, 2015). CENP-A recruitment via CENP-C further stabilizes the latter, as we found that CENP-C levels at the LacO array were higher in cells that had CENP-A (non-treated cells and in the IAA WO) compared to IAA-treated cells (Fig 5B–D).

We next tested which CENP-B domains were involved in CENP-C recruitment. Previous yeast two-hybrid analysis suggested that CENP-B's acidic domain interacts with CENP-C (Suzuki *et al*, 2004). We transiently expressed several CENP-B constructs that lack either the DNA Binding Domain (DBD), the acidic domain, or both. As positive and negative controls, we used CENP-B Full Length (FL) and H3.1 or CENP-T$^{\Delta C}$ (Gascoigne *et al*, 2011), respectively. As the DBD of CENP-B was shown to interact with CENP-A (Suzuki *et al*, 2004; Fujita *et al*, 2015), we performed these experiments in the absence of CENP-A (+IAA) to avoid any interference of CENP-A in CENP-C recruitment. In agreement with previous studies (Gascoigne *et al*, 2011; Hori *et al*, 2013), we could not observe CENP-C recruitment by H3.1 or ectopic CENP-T. Surprisingly, CENP-C was recruited at the CENP-B$^{\Delta acidic}$-LacI in a similar manner to that of FL or ΔDBD (Fig 5F). However, double deletion of both the DBD and the acidic domain almost completely prevented CENP-C recruitment to a level similar to that of CENP-T or the negative control H3.1 (Fig 5F). This remaining small fraction of CENP-C recruited to the LacO could be due to the presence of endogenous CENP-B that dimerizes with the CENP-B variants. We confirmed these results using pull-down assays with purified recombinant proteins (Appendix Fig S2H–J). Here, we observed direct interaction between GST-CENP-C (1–727) and $^{\Delta DBD}$CENP-B (Fig 5G). However, removal of the acidic domain in $^{\Delta DBD}$CENP-B abolished the interaction with CENP-C (Fig 5G). In summary, we concluded that both the acidic domain and the DBD of CENP-B are involved in CENP-A-independent recruitment and maintenance of CENP-C that, in principle, is capable to initiate the epigenetic centromere assembly loop mediated by CENP-A.

CENP-B marks native centromere position to promote *de novo* CENP-A/C reloading

Given the strong enrichment of CENP-B-LacI at the LacO array, it was unclear if the interaction with CENP-C is relevant for new CENP-A deposition at endogenous centromeres. In addition, CENP-

B-LacI at the LacO array could potentially cluster with endogenous centromeres. Therefore, we tested if CENP-B could promote centromere formation also at the native centromere position, where CENP-B levels are far lower compared to the LacI system. To test this, we generated a DLD-1 cell line in which both endogenous CENP-A and CENP-C can be rapidly depleted (and re-expressed) simultaneously using the auxin-inducible protein degradation system (CENP-A/C$^{OFF/ON}$; Appendix Fig S3A–C).

After CENP-A/C depletion and re-activation, we tested if both proteins were reloaded *de novo* to the centromere and if it was CENP-B-dependent (Fig 6A and B). Following CENP-A/C$^{OFF/ON}$, we observed reloading of both proteins at some CENP-B-positive

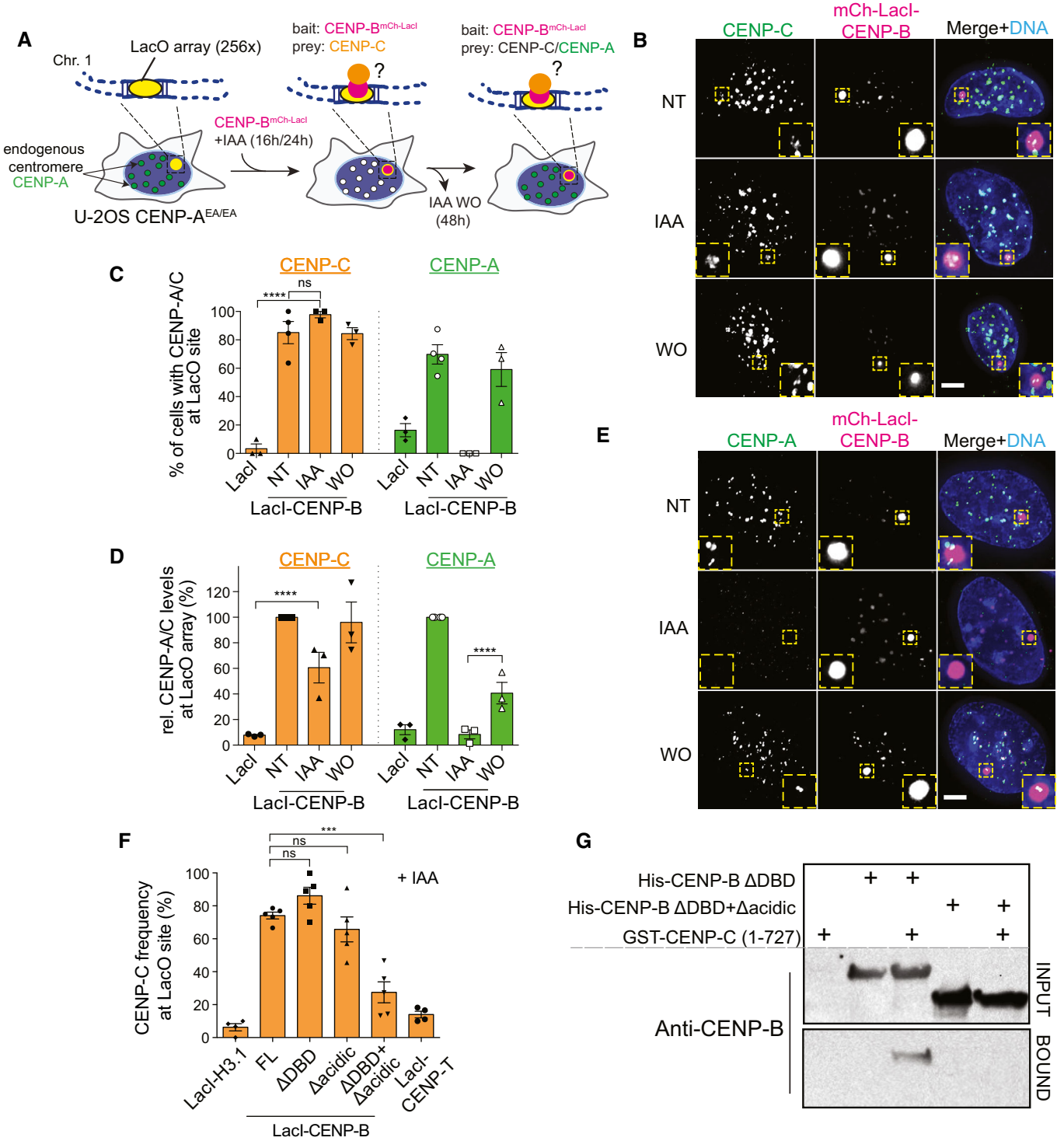

Figure 5.

Figure 5. Ectopic CENP-B is capable to recruit CENP-C independently of CENP-A at LacO arrays.

A Experimental schemes for B-F. LacI-CENP-B or LacI control (baits) was expressed into CENP-A$^{EA/-}$ lacO-tetO U-2OS cells. Immunostaining against CENP-C or CENP-A (preys) was performed following LacI-CENP-B transfection in untreated, IAA-treated, and IAA wash-out (WO) conditions.

B Representative immunofluorescence images showing CENP-C recruitment at the LacO array in the indicated conditions. LacO array is displayed in the insets. Scale bar, 5 μm.

C Bar plot showing frequency of CENP-C (orange) or CENP-A (green) recruitment to LacO array in the indicated conditions. Each dot represents one independent experiment (> 20 cell analyzed for experiment). Error bars represent SEM from 3 independent experiments. Unpaired *t*-test, ****$P < 0.0001$.

D Quantification of CENP-C (orange) or CENP-A (green) protein levels at the LacO array in the indicated conditions normalized to protein intensities in non-treated conditions at the mCherry-LacI-CENP-B-LacO array using CENP-A or CENP-C antibody. Each dot represents one independent experiment (> 20 cell analyzed for experiment). Error bars represent SEM from 3 independent experiments. Mann–Whitney test was performed on pooled single cell data of three independent experiments, ****$P < 0.0001$.

E Representative immunofluorescence images showing CENP-A recruitment to ectopic mCherry-LacI-CENP-B in the indicated conditions. LacO array is shown in the inset. Scale bar, 5 μm.

F Quantification of the frequency of CENP-C recruitment to LacO arrays by different LacI constructs. Error bars represent SEM from 5 independent experiments. Unpaired *t*-test, ***$P = 0.0001$.

G CENP-B immunoblot following GST pull-down experiments using GST-tagged CENP-C (1–727) as bait and with the indicated proteins as preys.

Source data are available online for this figure.

centromeres in ~30% of the cells (Fig 6C and D). CENP-A reloading under this condition was also observed by live cell imaging (Movie EV2 and Appendix Fig S3E) and CUT&RUN followed by qPCR (Fig 6E). We noticed that only a fraction of centromeres per cell show efficient reloading, as also demonstrated by the low CENP-A/C centromeric protein levels upon re-activation (Appendix Fig S3F). When CENP-A/C reloading did not occur at all centromeres, there was a detrimental impact on cell viability, differently to what we observed in cells in which only CENP-A is removed and re-activated (Appendix Fig S3G).

Despite only a fraction of centromeres show CENP-A/C reloading, our data indicate that the endogenous centromere position remains the hotspot for new centromere formation even in the absence of CENP-A and CENP-C. We next tested if partial *de novo* CENP-A/C reloading was CENP-B dependent. Upon downregulation of CENP-B by siRNA (Appendix Fig S3H), *de novo* CENP-A/C reloading was almost completely lost, as observed by IF and CUT&RUN–qPCR (Fig 6B–E), reduced to a similar level as that obtained by downregulating M18BP1 expression via siRNA (Fig 6B–D).

Altogether, our results show that, occasionally, CENP-B can initiate CENP-A/C deposition to maintain centromere position along with the canonical CENP-A deposition machinery (at least M18BP1-mediated) in cells in which CENP-A/C was simultaneously co-depleted.

CENP-B initiates the CENP-A self-assembly epigenetic loop by recruiting CENP-C at native human centromeres

We next wanted to identify the mechanism by which CENP-B promotes *de novo* CENP-A/C reloading at the centromere. Our results imply a model in which CENP-B drives the initiation of the epigenetic centromere assembly loop. This can be achieved either by direct recruitment of CENP-A via CENP-B-DBD (Okada *et al*, 2007; Fujita *et al*, 2015), or by direct recruitment of CENP-A via CENP-C that in turn interacts with components of the Mis18 complex (Moree *et al*, 2011; Stellfox *et al*, 2016). Alternatively, CENP-B could directly promote the recruitment of the Mis18 complex (Fig EV4A), although previous evidence argued that the M18BP1 complex is insufficient to recruit endogenous CENP-A at an ectopic site (Shono *et al*, 2015). To test this hypothesis, we measured the number of endogenous M18BP1 centromere foci in early G1 RPE-1 cells following rapid depletion of CENP-A, CENP-C, or co-deletion of CENP-A and CENP-B (Fig EV4B). CENP-A removal or depletion of CENP-B alone did not alter M18BP1 recruitment at centromeric regions, while CENP-A/CENP-B co-depletion led to a reduction in the total number of M18BP1 foci (Fig EV4B–D). Rapid and complete removal of CENP-C even further perturbed M18BP1 foci at most centromeres (Fig EV4C and D). Since CENP-C depletion showed the most drastic effect, and co-depletion of CENP-A/CENP-B lead to a strong, although not complete, loss of centromeric CENP-C signal (Hoffmann *et al*, 2016), we favor the model that CENP-C, but not CENP-B, promotes M18BP1 recruitment, as previously observed (Moree *et al*, 2011; Dambacher *et al*, 2012).

Our data emphasize that endogenous centromeric CENP-B can initiate the epigenetic self-assembly loop via CENP-C recruitment independently of CENP-A. Hence, we next dissected the temporal events that control centromere formation at endogenous CENP-B positive centromeres (Fig 7A). To do this, we developed a system to rapidly co-deplete CENP-A and CENP-C and separately induce the expression of either exogenous (e) CENP-A or CENP-C tagged with mRFP and a DHFR destabilization domain (Figs 7B and EV4E). The expression of ectopic eCENP-A or eCENP-C was placed under the control of a doxycycline-regulatable promoter and stabilized by addition of TMP molecule (Fig EV4E and F).

We first tested if eCENP-A can be loaded at the CENP-B-positive centromeres that lack preexisting CENP-A and CENP-C. We synchronized cells to be able to monitor eCENP-A loading in G1 prior to or after endogenous CENP-A/C removal by IAA (Fig EV4G). Surprisingly, we did not observe any eCENP-A loading when endogenous CENP-A/CENP-C was removed prior to its deposition, in contrast to control cells in which CENP-A/C removal was performed after eCENP-A loading (Fig 7C and D). The absence of eCENP-A loading to centromeric regions depleted of CENP-A/C was also confirmed by CUT&RUN–qPCR (Figs 7E and EV4H). This lack of signal was only partly explained by CENP-A reduced stability due to the absence of CENP-C (Falk *et al*, 2015, 2016), as even prolonged IAA treatment (24 h) in control cells to remove endogenous CENP-A/C did not abolish the enrichment of eCENP-A at centromeric regions (Fig EV4G and I).

Next, we tested the capacity of eCENP-C to be reloaded at the centromere in the absence of centromeric CENP-A/C. Here, we used asynchronous cells (Fig EV4J) as CENP-C loading is not restricted to early G1 (Hoffmann *et al*, 2016). In contrast to eCENP-A, we found that initial depletion of endogenous CENP-A/C did not prevent

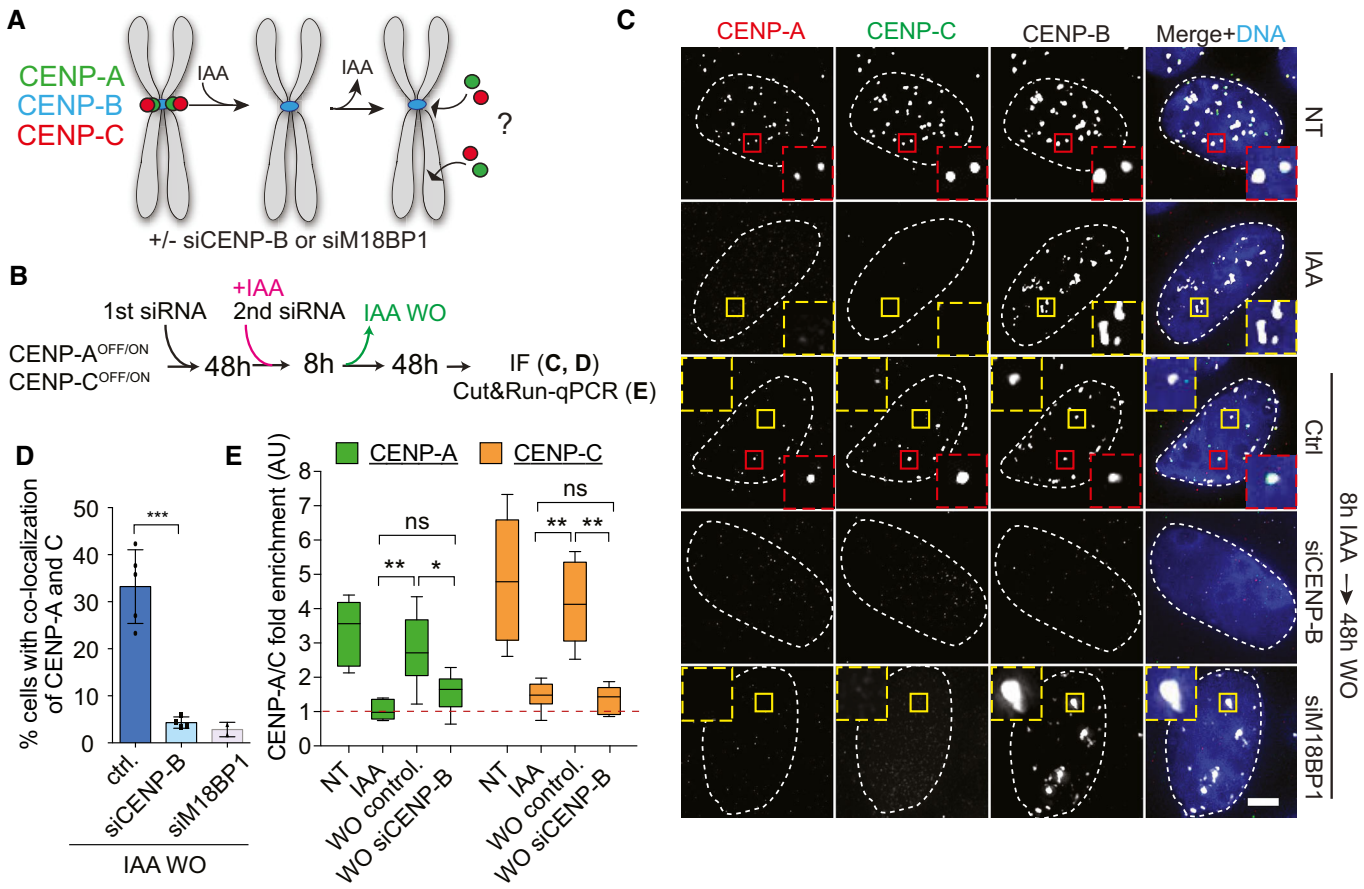

Figure 6. CENP-B drives *de novo* CENP-A and CENP-C assembly at endogenous centromeres.

A Schematic representation of experiments in B–E.

B Timeline of experiment in C-E.

C Representative immunofluorescence images showing CENP-A and CENP-C reloading in the indicated conditions. Cells with centromeric CENP-A/CENP-C are marked with a red dashed contour line, while a yellow contour lines mark cell without centromeric CENP-A. The centromere position is marked using immunofluorescence staining for CENP-B. White dashed lines contour DAPI stained nucleus of representative cells. Scale bar, 5 μm.

D Bar plot showing the percentage of cells with CENP-A and CENP-C co-localization after a CENP-A/C$^{OFF/ON}$ cycle in the indicated conditions. Error bars show SD from 5 independent experiments. Unpaired *t*-test, ***P = 0.0002. Each dot represents one experiment (> 30 cells analyzed for experiment).

E Box plot of CUT&RUN–qPCR for CENP-A (green) or CENP-C (orange). Box plot shows median, 25th and 75th percentiles, and whiskers show minimum and maximum values. Results from 3 independent experiments including combined data from qPCRs using alpha-satellite primers and primers binding at the centromere of chromosome 4. Enrichment is measured relative to the IgG control and normalized to Alu repeats. Mann–Whitney test, CENP-A: **P = 0.0087, *P = 0.0411, CENP-C: **P = 0.0022.

eCENP-C loading at CENP-B-positive centromeres in ~60% of interphase or mitotic cells (Figs 7F and G, and EV4J–L). As previously noted (Fig 6A–E), we observed only partial centromeric eCENP-C loading (Fig EV4L). We confirmed the ability of eCENP-C to reload at the centromere by CUT&RUN–qPCR in the absence of CENP-A reloading (Figs 7H and EV4M).

Altogether, our results show that CENP-C, but not CENP-A, can be loaded, at least partially, at centromeres that lack previously deposited CENP-A/CENP-C.

CENP-A-negative resting CD4$^+$ T cells re-assemble CENP-A *de novo* upon cell cycle entry

Our results imply that CENP-B provides memory of centromere identity. We next aimed to assess the physiological relevance of this mechanism. While dividing cells maintain CENP-A expression, terminally differentiated non-dividing cells lacking CENP-A have been described (Swartz *et al*, 2019). Subsets of differentiated lymphocytes are quiescent in the peripheral blood from healthy individuals, and they can re-enter the cell cycle upon activation through T Cell Receptor (TCR) activation. We hypothesized that a sub-population of circulating T lymphocytes may contain a fraction of CENP-A-negative cells, and they might re-acquire CENP-A expression and centromere deposition upon activation. We measured the level of CENP-A and CENP-B in resting, non-dividing CD14$^-$/CD4$^+$ T cells isolated from peripheral blood of healthy human donors (Fig EV5A). While all the analyzed CD4$^+$ T cells were CENP-B-positive, two distinct populations were detected based on their CENP-A expression, referred to as CENP-A^{high} and CENP-A^{low} (Figs 8A and EV5B). Next, we sorted CENP-A^{high} and CENP-A^{low} CD4$^+$ T cells to

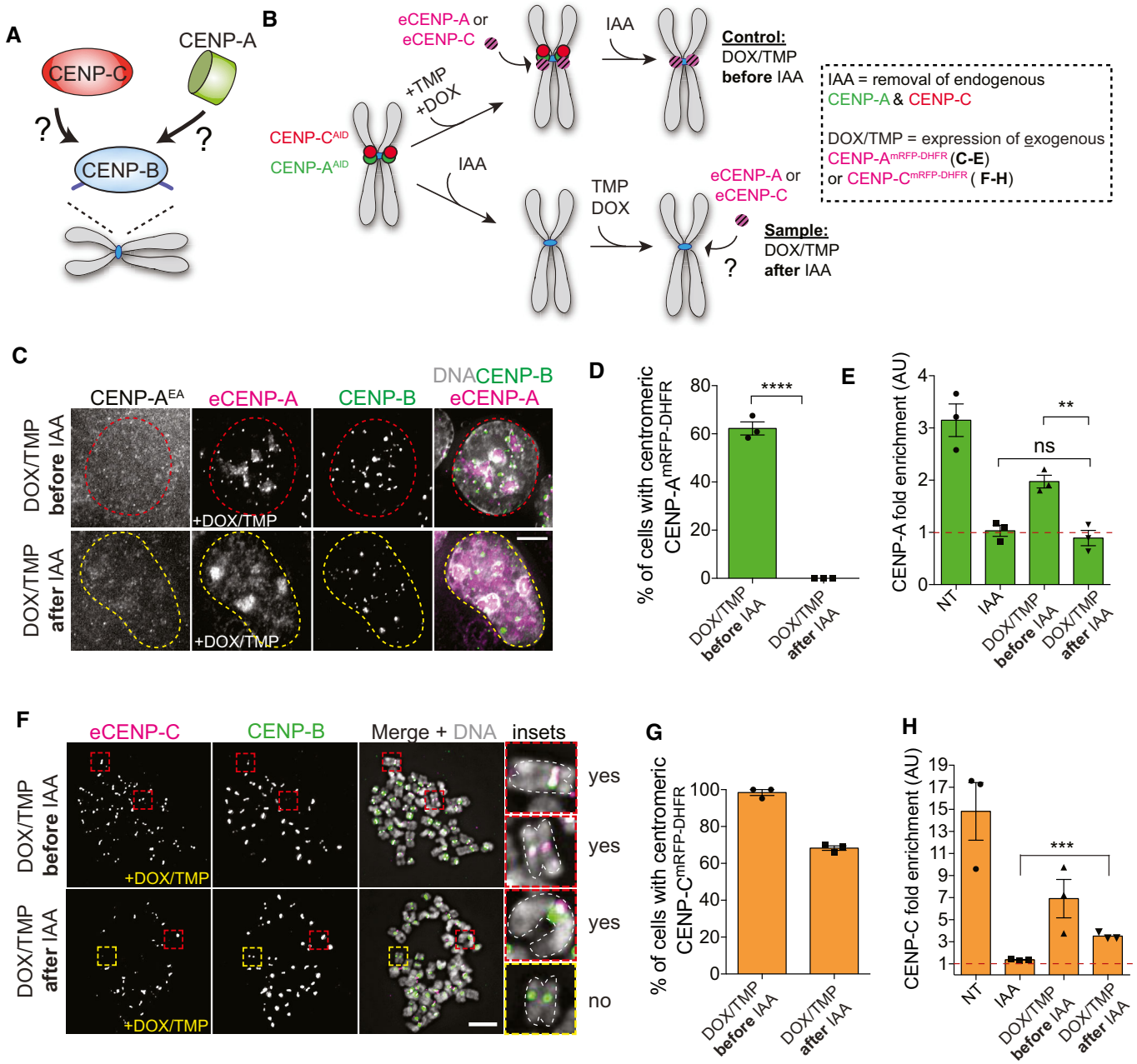

Figure 7. CENP-B is capable to initiate the CENP-A-mediated epigenetic loop via *de novo* recruitment of CENP-C at the native centromere.

A Schematic to illustrate the goal of this experiment.

B Schematic illustration of the experiments performed in C-H.

C Representative immunofluorescence images showing exogenous CENP-A$^{mRFP\text{-}DHFR}$ reloading in the presence (control), but not in the absence (sample) of endogenous CENP-A and CENP-C. Scale bar; 5 μm. Chromosomes with centromeric CENP-A are marked with a red dashed contour line, while a yellow contour line marks cell chromosome without centromeric CENP-A.

D Quantification of relative number of cells showing centromeric eCENP-A$^{mRFP\text{-}DHFR}$ in the indicated conditions. Error bars represent SEM from 3 independent experiments. Each dot represents one independent experiment with at least 30 cells per condition. Unpaired *t*-test, ****$P < 0.0001$.

E Bar plot of CUT&RUN–qPCR quantification using CENP-A antibody and primers binding at the centromere of chromosome 4. Enrichment is measured relative to the IgG control and normalized to Alu repeats. Error bars represent SEM from 3 independent experiments. Each dot represents one independent experiment. Unpaired *t*-test, **$P = 0.0048$.

F Representative immunofluorescence chromosome spreads showing reloading of exogenous eCENP-C$^{mRFP\text{-}DHFR}$ in the presence (control) and in the absence (sample) of endogenous CENP-A and CENP-C. Cells were arrested with colcemid for 3 h prior to spread. Cells with centromeric CENP-C are marked with a red dashed contour line, while a yellow contour line marks cell without centromeric CENP-C. Chromosomes in inset are highlighted using a white dashed line. Scale bar, 5 μm.

G Quantification of relative number of cells with eCENP-C$^{mRFP\text{-}DHFR}$ in the indicated conditions. Each dot represents one independent experiment with at least 30 cells per condition. Error bars represent SEM from 3 independent experiments.

H Bar plot of CUT&RUN–qPCR results using CENP-C antibody and primers binding at the centromere of chromosome 4. Enrichment is measured relative to the IgG control and normalized to Alu repeats. Each dot represents one independent experiment. Error bars represent SEM from 3 independent experiments. Unpaired *t*-test, ***$P = 0.0003$.

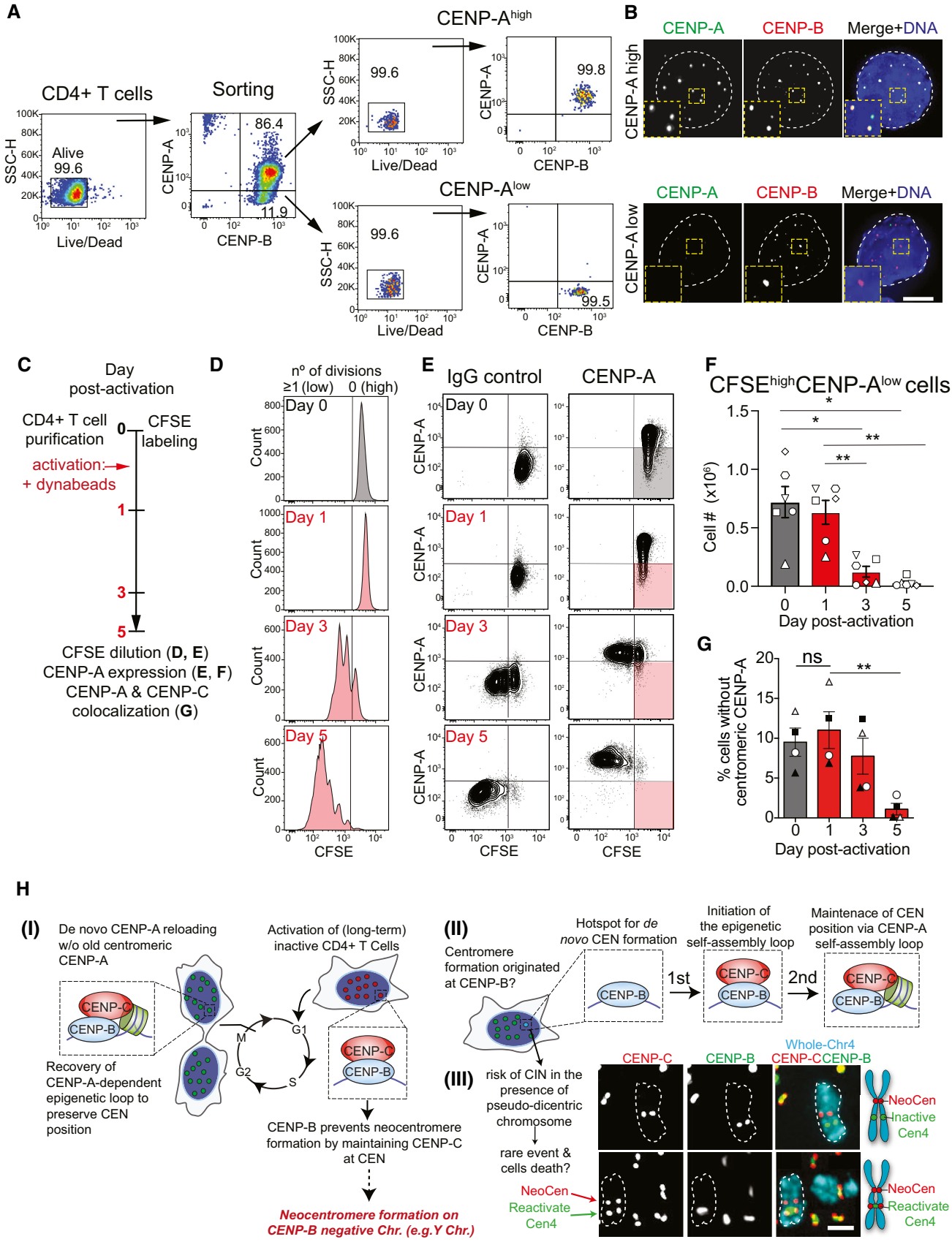

Figure 8.

Figure 8. Centromere identity is maintained in resting CENP-A-deprived CENP-B/C positive CD4$^+$ T cells.

A Gating strategy for the sorting of freshly purified resting human CD4$^+$ T cells based on CENP-A expression. Dead cells were excluded (first plot) using Fixable Viability Dye eFluor 780, and CENP-A^{high} and CENP-A^{low} cells (both CENP-B$^+$) were sorted (second plot). Post-sort analysis of each population is then shown (third and fourth plots).

B Representative images of sorted CD4$^+$ T cells with high or low CENP-A level. The nucleus is contoured by a white dashed line. Scale bar, 5 μm.

C Schematic representation of the analysis of CENP-A expression over time in CD4$^+$ T cells, shown in D-G. T cells were activated with anti-CD3/anti-CD28-coated beads.

D Tracking of cell division by CFSE dilution. The black line separates cells that have not divided (no of div = 0, CFSE high) from those that have undergone at least one division (no of div ≥ 1, CFSE low).

E CENP-A expression and CFSE dilution. Black lines were set based on CENP-A isotype control and CFSE maximal staining at day 0 (cells in shaded quadrants are CFSE-high/CENP-A-low). One representative donor is depicted.

F Absolute number of CFSE-high/CENP-A-low CD4$^+$ T cells (shaded gate in E). Symbols represent individual donors. Error bars represent SEM from 6 independent donors. One-way ANOVA, multiple comparisons, $n = 6$. *$P < 0.05$; **$P < 0.01$.

G Frequency of cells without centromeric CENP-A determined by immunofluorescence microscopy before and post-activation. Symbols represent individual donors, $n = 4$. Error bars represent SEM from 4 independent donors. Unpaired t-test: **$P = 0.0064$.

H Model of the role of CENP-B in the maintenance of centromere identity. I-III: See text for details. In III: (top) representative image of a pseudodicentric chromosome in PD-NC4 cells with an active (red) and inactive (green) centromere bound by CENP-C and CENP-B, respectively; (bottom) example of a rare centromere re-activation in which the inactive (red) centromere gains CENP-C binding capacity. White dashed lines contour representative chromosomes. Schematic to the right illustrates the observed CENP-C and CENP-B localization patterns on a chromosome.

investigate CENP-A localization. While in CENP-A^{high} cells CENP-A colocalized with centromeric CENP-B, in most CENP-A^{low} cells CENP-A was undetectable or barely detectable at CENP-B-marked centromeres (Figs 8B and EV5C and D). In contrast, CENP-C localized at these CENP-A-depleted centromeres (Fig EV5E). This result prompted us to investigate CENP-A expression and localization upon T-cell activation (Fig 8C). To track the number of cell divisions across time, purified CD4$^+$ T cells were labeled with the fluorescent dye CFSE (Fig 8D). In undivided cells (CFSE^{high}), we observed a gradual increase in CENP-A expression from day 1 to day 3 upon T-cell activation (Figs 8E and EV5F), consistent with the exit from quiescence and re-entry in the cell cycle (Figs 8D and E, and EV5F). The frequency of dead cells did not increase between day 1 and day 3 (Fig EV5H), suggesting that CENP-A^{low} T cells were not lost as a result of compromised viability. In cells that had divided at least once (CFSE^{low}, day 3 to day 5), the CENP-A level was high and homogenous (Figs 8D and E, and EV5F). At day 3, only the remaining population that had not yet divided (div 0) contained cells expressing lower levels of CENP-A, compared to cells that had divided (Fig EV5I and J). These results were consistent across independent blood donors (Figs 8F and EV5G and J) and were confirmed by immunofluorescence analysis (Figs 8G and EV5K). Our data thus suggest that CENP-A^{low} T lymphocytes convert into CENP-A^{high} cells upon T-cell activation before cell division. Overall, we conclude that a physiologic sub-population of quiescent resting human CD4$^+$ T cells expresses CENP-B and CENP-C, but lacks detectable centromeric CENP-A. Upon cell cycle entry, CENP-A is reloaded at endogenous centromeres, in agreement with the essential role of CENP-B/CENP-C in the maintenance of centromere identity.

Discussion

In this work, we identify CENP-B as a key contributor to maintain centromere position together with CENP-A (Fig 8H$_I$). By preserving a critical level of CENP-C at native centromeres, CENP-B provides memory for maintenance of native human centromeres by promoting *de novo* CENP-A assembly. This has a physiological impact in cells that have temporarily lost CENP-A (e.g., a sub-population of resting CD4$^+$ T cells) where the CENP-B/CENP-C connection is key to preserving the original centromere identity. Additionally, under selective pressure, neocentromere-like elements form at CENP-B-negative centromeres. We demonstrated that CENP-B bound to centromeric DNA can trigger the recruitment of CENP-C, not only at ectopic LacO site, but also at native centromeres (Fig 8H$_{II}$). We show that CENP-C is a key factor for CENP-A loading which, subsequently, initiates the maintenance of centromere position in a CENP-A-dependent manner. While CENP-C has been mainly described as the reader of the epigenetic mark CENP-A, now we have demonstrated its capability to recognize and mark centromere position via CENP-B and independently of CENP-A. Moreover, we showed that CENP-A itself, in the absence of CENP-C, lacks this ability to reinstate centromere memory. In contrast to previous models, our observations suggest that *de novo* centromere formation is likely initiated by a critical level of CENP-C rather than CENP-A (Fig 8H$_{II}$). However, our data still emphasize the importance of the centromeric self-assembly loop to efficiently maintain centromere position for indefinite cell cycles, a function that cannot be fulfilled exclusively by CENP-B and CENP-C themselves. This is in agreement with the well-studied essentiality of CENP-A in proliferating somatic cells in all CENP-A-containing species studied so far (Fukagawa & Earnshaw, 2014; McKinley & Cheeseman, 2016; Stankovic & Jansen, 2017).

Our data have several implications. First, as CENP-A also incorporates outside the canonical centromeric sites (Bodor *et al*, 2014; Nechemia-Arbely *et al*, 2019), we propose that CENP-B is required to prevent neocentromere formation by preserving CENP-C at the original centromere location and favoring the maintenance of centromere identity in a CENP-C-dependent manner (Fig 8H$_I$). This is even more critical in the event of CENP-A up-regulation, as observed in some types of cancer, although to date is still unclear how massive CENP-A mis-incorporation promotes the emergence of genome instability (Barra & Fachinetti, 2018). Certainly, in contrast to what has been observed in flies (Heun *et al*, 2006; Olszak *et al*, 2011), ectopic CENP-A is unable to drive neocentromere formation in human cells. This could be explained by the lack of CENP-C-mediated nucleosome protection mechanism of ectopic CENP-A during DNA replication (Nechemia-Arbely *et al*, 2019) that we argue

is strongly supported by CENP-B. Furthermore, we have proven that, under selective pressure, neocentromere-like elements can form on the CENP-B-deficient centromere of the Y chromosome (Fig 4).

The contribution of the CENP-B/CENP-C connection to centromere identity is most relevant at CENP-A-depleted centromeres (Fig 8H$_{I}$). We identified a population of resting CD4^{+} T cells characterized by low CENP-A expression with undetectable localization at centromeres (Fig 8A and B). The origin and properties of T cells lacking CENP-A warrants further study. We hypothesize that CENP-A loss under physiological conditions could be a consequence of prolonged cell cycle withdrawal, a feature of quiescent cells. This suggests the inability to reload CENP-A during quiescence, a phenomenon recently described (Swartz *et al*, 2019). Importantly, this loss is reversible in CD4^{+} T cells and we find that resuming the cell cycle restores CENP-A expression and centromere localization. In this scenario, upon cell activation, T cells are more likely to reactivate CENP-A transcription during G2 (Shelby *et al*, 1997) and to reload it at mitotic exit via its canonical pathways (Zasadzińska & Foltz, 2017), as the absence of CENP-A in the first mitosis can be tolerated (Hoffmann *et al*, 2016). This type of *de novo* CENP-A reloading was also observed in our CENP-A$^{OFF/ON}$ system using human cell lines as we found full recovery of centromeric CENP-A level within one (Fig EV1B and C) or two cell cycles (Fig 1). This suggests the existence of a quantitative transmission mechanism, likely determined by CENP-A expression levels, that preserves the number of CENP-A molecules independently of the presence of previously deposited CENP-A. In T cells, one cell cycle was sufficient to recover full and homogenous CENP-A expression, irrespective of the initial fraction of CENP-A-low cells among independent donors. This demonstrates that the amount of previously deposited CENP-A molecules is not the key determinant of total centromere CENP-A. A complete turnover of all preexisting CENP-A molecules has been only previously observed in holocentric organisms (Gassmann *et al*, 2012). Our findings further demonstrate that post-translational modifications on preexisting centromeric CENP-A are not essential to guide new CENP-A deposition at the centromere in contrast to previously described models (Niikura *et al*, 2015, 2016).

Our results also show that endogenous CENP-B level enables centromere formation via CENP-C recruitment (Fig 8H$_{II}$). This finding has implications for the mechanisms that drive HAC formation via CENP-B, as we dissected the temporal events necessary for maintenance of centromere position. A previous report proposed that CENP-B promotes HAC formation via direct recruitment of CENP-A (Okada *et al*, 2007), since, to a certain extent, they stabilize each other (Fachinetti *et al*, 2015; Fujita *et al*, 2015). However, our data on ectopically tethered CENP-B and at native centromeres show that this interaction appears insufficient to load and stabilize CENP-A in the absence of CENP-C (Fig 7C–E and Appendix Fig S2C–G). Importantly, CENP-C is a key factor for centromere formation as it is both able to recruit CENP-A via the Mis18 complex (Moree *et al*, 2011; Dambacher *et al*, 2012; Stellfox *et al*, 2016; Pan *et al*, 2017) and stabilize it (Falk *et al*, 2015, 2016). Interestingly, the Mis18 complex was not sufficient to mediate detectable endogenous CENP-A assembly when tethered to an ectopic location (LacO) (Ohzeki *et al*, 2019), reinforcing the importance of CENP-C to maintain centromere position. However, our data do not entirely rule out a contribution of centromere components other than CENP-C to stabilize the Mis18 complex in human centromeres.

Finally, the existence of stably inherited pseudodicentric neocentric chromosomes—in which both the non-repetitive neocentromere bound by CENP-A and the inactive centromeric locus carrying satellite DNA and CENP-B are found on the same chromosome [e.g. PD-NC4 cells (Amor *et al*, 2004)]—disfavors the notion that CENP-B initiates centromere formation. In this scenario, the presence of ectopic CENP-B should represent a threat for the cells as it can occasionally lead to a dicentric chromosome. Indeed, we sporadically observed the spontaneous re-activation of the inactive native centromere in PD-NC4 cell line and the formation of a dicentric chromosome (Fig 8H$_{III}$). However, in these cells the abundance of repetitive DNA and CENP-B at the inactive centromere was particularly low (Fachinetti *et al*, 2015), perhaps reducing its ability to promote centromere formation via CENP-C recruitment. The potential to become a dicentric chromosome could further explain why the occurrence of pseudodicentric chromosomes remains a very rare event and that CENP-B only inefficiently promotes centromere formation on HACs (Ohzeki *et al*, 2002; Okada *et al*, 2007). Interestingly, to date, 3 out of 8 cases of described pseudodicentric neocentric chromosomes in humans occur on the Y chromosome (Marshall *et al*, 2008) where centromere re-activation is predicted to be less frequent due to lack of CENP-B. Previous reports have suggested that CENP-B is removed from non-centromeric regions via its chaperone Nap1 (Tachiwana *et al*, 2013). Considering our findings, such regulation appears also to be important to prevent CENP-B-driven centromere formation outside of alpha-satellite DNA.

Altogether, our data suggest cooperation of CENP-A/CENP-B/CENP-C in maintenance of centromere position and function. CENP-C, via CENP-B, is the initiation factor for new centromere formation capable to promote *de novo* CENP-A deposition, that in turn stabilizes CENP-C in a temporal manner. What causes the heterogeneity of CENP-B-mediated CENP-C recruitment remains to be identified. As the percentage of cells that reload CENP-C doubles following ectopic CENP-C expression (Fig 7G), it is possible that the inefficient reloading is due to low CENP-C protein levels following IAA WO. In this regard, the importance of CENP-C for endogenous CENP-A loading was previously observed at ectopic chromatin-integrated LacO sites (Hori *et al*, 2013; Shono *et al*, 2015). However, CENP-C protein levels at these ectopic sites are tremendously higher compared to the native centromere. As protein level recovers gradually over time following IAA wash-out, this can explain why we initially failed to identify rapid new CENP-C loading (within 3 h) at endogenous centromeres in the absence of CENP-A (Hoffmann *et al*, 2016). CENP-C is also absent at the CENP-B-bound inner centromere during metaphase. Possibly, the chromatin environment or post-translational modifications might also regulate CENP-C recruitment. Concerning this aspect, the acidic domain of CENP-B was recently described to function as an interface for several chromatin remodeling proteins with either chromatin compaction or decompaction activities (Otake *et al*, 2020). Although the precise regulation of these CENP-B-mediated chromatin alterations remains unclear, chromatin compaction could impair CENP-C recruitment and thus explain partial CENP-C recruitment.

Another question that remains to be elucidated is the role of CENP-I in centromere formation as it was shown to recruit CENP-A at an ectopic site (Hori *et al*, 2013; Shono *et al*, 2015) and to display

an extended localization profile compared to the other CCAN proteins in a similar, but not identical pattern to CENP-B (Kyriacou & Heun, 2018). However, *in vitro* assays favor the hypothesis of a cooperative binding between CENP-I and the CCAN likely via a direct interaction with CENP-C (Klare *et al*, 2015; McKinley *et al*, 2015; Weir *et al*, 2016; Pesenti *et al*, 2018) that in turn promotes and stabilizes centromeric CENP-A.

Finally, our model does not exclude that CENP-B and repetitive DNA could maintain the centromere in a manner that is independent of the direct interaction with CENP-B and CENP-C. A recent computational study suggested that CENP-B induces the formation of specific non-B DNA structure (Kasinathan & Henikoff, 2018) that could potentially facilitate CENP-A incorporation. Interestingly, BACs containing centromeric DNA favor CENP-A assembly in contrast to non-centromeric DNA (Aze *et al*, 2016). Non-B DNA structures are also observed at CENP-B-free centromeres (neocentromeres and the Y chromosome) and could explain the formation of *de novo* centromere on some types of DNA in a HAC formation assay (Logsdon *et al*, 2019). In support of this hypothesis, our data on CENP-A reloading at the Y chromosome show that the alpha-satellite DNA sequences provide CENP-B independent features that favor centromere re-formation. More studies are needed to shed light on the centromere DNA secondary structures and their possible role in centromere biology. Interestingly, in *S. pombe*, centromere DNA inherently destabilizes H3 nucleosomes to favor CENP-A deposition (Shukla *et al*, 2018). Previous studies have also reported that CENP-C has DNA binding activity, that could potentially promote CENP-C loading to site of *de novo* centromere formation, although its DNA sequence specificity remains uncertain (Sugimoto *et al*, 1994; Yang *et al*, 1996; Politi *et al*, 2002; Xiao *et al*, 2017). Additionally, the alpha-satellite locus bears marks of active transcription (Sullivan & Karpen, 2004) and satellite transcripts might play a direct role in centromere formation by mediating CENP-A and CENP-C incorporation (Bergmann *et al*, 2010; Chan *et al*, 2012; Quénet *et al*, 2014; Chen *et al*, 2015; McNulty *et al*, 2017; Bobkov *et al*, 2018). CENP-B might play an additional role in transcript regulation possibly by competing with DNA methylation and methylated DNA binding proteins at CENP-B boxes (Scelfo & Fachinetti, 2019). Lastly, CENP-B was proposed to act as a chromatin regulator by directly modulating heterochromatin formation (Okada *et al*, 2007; Morozov *et al*, 2017). Indeed, the acetyltransferase KAT7 via M18BP1 has been implicated in CENP-A deposition (Ohzeki *et al*, 2016).

Future studies will be important for defining the interplay among DNA sequence, transcription, and epigenetic modifications in establishing and maintaining centromere identity via CENP-B and CENP-C.

Materials and Methods

Cell culture

Cells were cultivated at 37°C in a 5% CO_2 atmosphere. Flp-In TRex DLD-1 cells and U-2OS 2-6-3 R.I.K LacO cells (Janicki *et al*, 2004) were maintained in Dulbecco's modified essential medium (DMEM) medium containing 10% tetracycline free Fetal Bovine Serum (FBS, Pan Biotech). U-2OS cells were cultured with 0.1 mg/ml hygromycin (Invitrogen). Immortalized hTERT RPE-1 cells were maintained in DMEM:F12 medium containing 10% Fetal Bovine Serum (BioSera), 0.123% sodium bicarbonate, and 2 mM L-glutamine.

IAA (I5148; Sigma) dissolved in ddH_2O was used at 500 μM, doxycycline (1 μg/ml), TMP (10 μM), reversine (0.5 μM), colcemid (0.1 mg/ml, Roche), palbociclib (1 μM), G418^{TM} (0.3 mg/ml, Gibco^{TM}), Flavopiridol (5 μM, Sigma), and NM-PP1 (5 μM, Sigma). IAA was washed-out three times using culture medium. Efficient IAA removal was ensured by first repeating the washes after 15 min and second after 30 min to allow excess compound to diffuse from cells. For DOX/TMP wash-outs, cells were additionally detached (TrypLE^{TM}, Gibco), washed by centrifugation, and then re-seeded on glass slides in normal culture medium.

Gene targeting

Gene targeting was performed using either CRISPR/Cas9 to target CENP-B (5′-CACCGCGCGATCTCGCCCTTGCGCAAAC-3′) and RPS4Y (guide RNAs: 5′-caccgTCCGTCGCAGAGTTTCGCCA-3′) or TALENs to target CENP-A (5′-GTCATGGGCCCGCGCC-3′ and 5′-GGCCC CGAGGAGGCGCA-3′) and CENP-C (5′-GAGGAAAGTGTTCTTC-3′ and 5′-GGTTGATCTTTCATC-3′), as described previously (Fachinetti *et al*, 2015; Hoffmann *et al*, 2016; Hoffmann & Fachinetti, 2018). Here, we introduced a mini-AID-LoxP-P2A-neomycin-LoxP sequence at the C terminus of the CENP-C gene and a mCherry sequence at the C terminus of the CENP-B gene using modified pUC57 plasmids harboring the inserts and homology arms (assembled via Gibson cloning). A start codon-deprived neomycin resistance cassette was integrated in frame with the start codon of the non-essential RPS4Y gene on chromosome Y. Cells were selected either by neomycin treatment (0.3 mg/ml) or by FACS sorted as described previously (Hoffmann & Fachinetti, 2018). Successful integration was confirmed by PCR, immunoblot, and/or immunofluorescence microscopy. Analog sensitive (AS) CDK1 expressing RPE-1 cells were generated using a one-shot isolation strategy as described in Saldivar *et al*, 2018. In brief, puromycin-sensitive RPE-1 CENP-A$^{EA/EA}$ was transfected with a CDK1^{AS} expression vector, a sleeping beauty transposase expression vector, and an endogenous CDK1 inactivation vector (0.5 μg for each plasmid) using nucleofection (Lonza). Successful integration of CDK1^{AS} gives rise to puromycin (5 μg/ml) resistance. G2 phase cell cycle block was confirmed in selected and isolated clones by FACS analysis after overnight NM-PP1 (5 μM) treatment.

Generation of stable cell lines

The FRT/Flp-in system was used to generate stable cell lines as described previously (Fachinetti *et al*, 2013). Briefly, we integrated cDNA of carboxy-terminal tagged CENP-B^{mcherry} and CENP-C$^{DHFR-RFP}$ as well as amino-terminal tagged CENP-A$^{DHFR-RFP}$ or CENP-A$^{EYFP-AID}$ into a pcDNA5/FRT plasmid harboring a promoter and start codon lacking hygromycin resistance cassette and co-transfected this plasmid with a pOG44 plasmid (Flp-recombinase) in a 9:1 ratio into Flp-In TRex DLD-1 cells using FugeneHD (Promega). Correct integration of the insert at the isogenic FRT site gives rise to hygromycin resistance. After selection (0.3 mg/ml hygromycin, Invitrogen), single clones were isolated and tested for successful integration by immunofluorescence microscopy.

os-TIR1-9-myc was integrated using a recombinant retrovirus as described previously (Holland *et al*, 2012). Single cells were isolated using 5 μg/ml puromycin.

siRNA, transient transfections, EdU staining, and colony formation assay

Lipofectamine RNAiMax (Invitrogen) was used to introduce siRNAs as described previously (Fachinetti *et al*, 2013). siRNA SMARTpool against luciferase, M18BP1, CENP-B, and CENP-C was purchased from Dharmacon. siRNA pools against HJURP and DAXX were a kindly gift from the G. Almouzni laboratory (Lacoste *et al*, 2014). Lipofectamine RNAiMAX and siRNAs were mixed in serum-free OptiMEM (Gibco™).

LacI constructs were transfected into U-2OS cells using FugeneHD (Promega) following the manufacturer's instructions. FugeneHD and plasmids were mixed in serum-free OptiMEM. For this study, we generated different LacI-CENP-B constructs: HA-LacI or mCherry-LacI-CENP-B$^{full\text{-}length}$, HA-LacI-CENP-B$^{\Delta acidic}$ (1–405; 539–599), HA-LacI-^{NLS}CENP-B$^{\Delta DBD}$ (125–599), and ^{NLS}CENP-B$^{\Delta DBD + \Delta acidic}$ (125–405; 539–599) using Gibson assembly cloning. Plasmids for HA-LacI-H.3.3 and mCherry-LacI control constructs were kindly gifts from B. Black laboratory. CENP-T (1–374) and LacI-NLS (Gascoigne *et al*, 2011) were purchased from Addgene.

EdU click labeling was performed using Click-iT® labeling technologies (Thermo Fisher Scientific), and colony formation assays were performed as previously described (Barra *et al*, 2019).

Immunoblotting

Cell pellets were suspended in protein sample buffer, and samples were separated by SDS–PAGE, transferred onto nitrocellulose membranes (Bio-Rad), and revealed with the following antibodies: DM1A (α-tubulin, 1:5,000), CENP-A (1:1,000; Cell Signaling), GFP (1:1,000; Chromotek), HJURP (1:1,000; a kindly gift from D. Foltz), DAXX (a kindly gift from G. Almouzni), CENP-B (1:1,000; Abcam), GAPDH (1:10,000; Abcam), CENP-C (a kindly gift from I. Cheeseman and B. Black), and Vinculin (1:2,000, Sigma).

Immunofluorescence, chromosome spreads, IF-FISH, and live cell microscopy

Cells were fixed in 4% formaldehyde 0.1% Triton X-100 at room temperature for 10 min or in methanol at −20°C for 15 min and subsequently blocked in blocking buffer (2.5% FBS (v/v), 0.2 M glycine, 0,1% Triton X-100 (v/v) in PBS) for 30 min at room temperature or overnight at 4°C. Primary antibodies were incubated in blocking buffer for 2 h at room temperature. The following antibodies were used as follows: CENP-A (1:1,000; clone 3-19, ENZO, ref. ADI-KAM-CC006-E), CENP-C (1:1,000; CliniSciences, ref. PD030PD030 CliniSciences), CENP-B (1:1,000; Abcam, ref. ab25734), ACA (1:500; Antibodies), DM1A (α-tubulin, 1:2,000), HA (1:500; Institut Curie antibody platform), CENP-A (1:1,000, ref. #2186S, Cell Signaling), GFP and RFP booster (1:200, Chromotek), and APC-CD4 (1:50, ref. 555349, BD). Immunofluorescence in combination with fluorescence *in situ* hybridization (FISH) was performed as described previously(Dumont *et al*, 2020). Images of DAPI counterstained and immuno-/FISH-stained cells were collected using a Deltavision Core system (Applied Precision). If necessary, microscope stage coordinates were recorded for sequential FISH after immunofluorescence microscopy. For M18BP1 staining in hRPE-1, cells were fixed in methanol (−20°C) and extracted prior to blocking (in BSA) as previously described (Fachinetti *et al*, 2013). M18BP1 antibody was a kind gift from Paul Maddox, University of North Carolina. All secondary antibodies used for immunofluorescence microscopy were purchased from Jackson Immuno Research. After immunostaining, cells were DAPI counterstained and mounted using anti-fading reagent (Life technologies).

Movies of live cell were acquired using Deltavision Core system (Applied Precision) as described previously (Hoffmann *et al*, 2016). Cells were grown on high optical quality plastic slides (ibidi) for this purpose.

Single molecule microscopy

For single molecule microscopy (SMM), cells were seeded on optical quality glass-bottom dishes (FluoroDish™, World Precision Instruments). SMM was performed under conditions of 37°C and 5% CO_2 using a Tokai Hit heating system on an epifluorescence inverted microscope (IX71, Olympus). A Highly Inclined and Laminated Optical sheet (HILO) configuration was employed to reduce background fluorescence and enable the detection of single molecules (Tokunaga *et al*, 2008). Specifically, a 500-mm achromatic lens was used to focus the beam at the back focal plane of a 150× objective (UApo N 150× TIRF 1.45 NA, O.I., Olympus, France). A metallic mirror on a translation stage was used to displace the focal point of the beam from the center of the back focal plane of the objective and determine the angle of the beam. A slit allowed us to regulate the thickness of the HILO illumination. Illumination was performed using a 488-nm laser (488LM-200, ERROL, France) and a 564-nm laser (Sapphire 561, Coherent, Santa Clara, CA, USA). Illumination was controlled by an acousto-optical tunable filter (AOTFnC-400-650-TN, A&A Optoelectronic, France). A quad-band dichroic mirror (FF409/493/573/652-Di02-25 × 36, SEMROCK) was used to separate emission light from excitation light. The use of a quad band dichroic mirror led to small, but significant excitation of mCherry molecules using 488-nm laser. To block this signal, an additional 520/70 emission filter (SEMROCK) was used when illumination with the 488-nm laser was applied. Images were recorded using an EM-CCD camera (iXonEM DV860DCS-BV, Andor, Ireland) run in frame-transfer mode using a 10-ms time interval for a total of 2,000 frames. In case of overexpression of the GR^{EYFP} protein, the signal was bleached until individual fluorescence could be distinguished. To capture a single molecule of CENP-A^{EYFP} and avoid bleaching, great care was taken to avoid any illumination of the cell prior to the recording of the images. To that end, the CENP-B^{mcherry} signal was used to obtain proper focus on the centromeres prior to imaging of CENP-A^{EYFP}. Post-acquisition, integrated densities at the centromere or of single GR^{EYFP} spots were determined by manually drawing a 6 × 6-pixel square around the centromere marked by CENP-B^{mcherry}/CENP-C$^{AID\text{-}mcherry}$ or GR^{EYFP} spots using the software FIJI. For background corrections, we drew a bigger square (8 × 8-pixel) and generated a band of 1 pixel width that surrounds the first 6 × 6 pixel square as illustrated in Fig EV2D. The integrated density of the background band was subtracted from the integrated density of the inner square.

CUT&RUN sequencing and CUT&RUN–qPCR

CUT&RUN was performed according to the procedure reported by Skene and Henikoff (2017) (Skene & Henikoff, 2017) starting from one million cells and using anti-CENP-A (Ozyme, 2186S), anti-CENP-B (Abcam, ab25734), or anti-CENP-C (Abcam, ab33034) antibodies. Rabbit IgG isotype control antibodies (Thermo Fisher, 10500C) were used for background detection, and spike-in with yeast DNA was performed to allow comparison across samples (Skene & Henikoff, 2017). Illumina sequencing library was prepared using the Illumina TruSeq ChIP Library Preparation Kit according to the manufacturer's instructions. Sequencing was performed with an Illumina HiSeq 2500 system. qPCR was performed using the Light-Cycler 480 (Roche) system with primers reported below. Fold enrichment at centromeres was calculated using alpha satellite or D4Z1 primers, with the ΔΔCt method. The rabbit IgG isotype sample was used as control sample, and normalization was performed to the Ct values from the ALU repeat primers.

Target	Reference	Forward	Reverse
Alpha satellite	Hoffmann *et al*, 2016	TCCAACGAAGG CCACAAGA	TCATTCCCACAAA CTGCGTTG
D4Z1	Contreras-Galindo *et al*, 2017	CTGTAGTATCTG GAAGTGGACATT	CTGTAGTATCTGGAA GTGGACATT
ALU repeat	Lou *et al*, 2015	GATCTCGGCTC ACTGCAAG	GTGAAACCCCGTCTC TACTAAAAA

Bioinformatic analysis

Read mapping was performed as previously described (Dumont *et al*, 2020). Briefly, reads were mapped using the BWA-MEM algorithm of the BWA software package (Li & Durbin, 2009; preprint: Li, 2013) on the human reference genome GRCh38.p12 which includes centromere reference models (Miga *et al*, 2014; Nechemia-Arbely *et al*, 2017; Schneider *et al*, 2017).

To generate the full centromere coverage plot of Fig 2B, CENP-A CUT&RUN reads were normalized to the IgG control reads using bamCompare tool from the deepTools2 package (Ramírez *et al*, 2016) with the operation set to "ratio". Peak calling was performed using SICER1.1. (Xu *et al*, 2015). The centromeric peaks from the untreated and the auxin wash-out CENP-A CUT&RUN samples were compared using UCSC table browser (Karolchik *et al*, 2004) in two ways: first (Fig 2D) by counting the number of peaks overlapping by at least 20% of their length; second (Fig 2E) by measuring the total length in megabases of all the overlaps between untreated and auxin wash-out samples.

Read mapping to HOR arrays was carried out as previously described (Dumont *et al*, 2020). Briefly, the reads mapped on the centromere reference models of GRCh38 were extracted using samtools (Li & Durbin, 2009) and mapped with BWA-MEM on a reference composed of 64 centromeric HOR array consensus sequences (Nechemia-Arbely *et al*, 2019). Due to the high similarities between the HOR sequence of acrocentric chromosomes 13, 14, 21, and 22, reads could not be specifically assigned to these centromeres and they were excluded from the analysis. Read counts for cen1+5+19, cen16, cen2, and cen18 were corrected as previously described (Dumont *et al*, 2020), and each value was normalized to the total read number and to the spike-in control. Table EV1 lists normalized read counts for each HOR consensus sequence, excluding acrocentric chromosomes 13, 14, 21, and 22.

IF-FISH chromatin fiber

Cells were harvested for extended chromatin fiber preparation as previously described (Sullivan, 2010). Briefly, cells were harvested by trypsinization and washed in 1× PBS before dilution to 1×10^5 cells/ml and swelling in hypotonic buffer (1:1:1 75 mM KCl: 0.8% sodium citrate: dH_2O) for 10 min. Cells were cytospin using a Shandon Cytospin 4 (Thermo Fisher) onto slides at 800 rpm. Slides were then immersed in lysis buffer (25 mM Tris–HCl, pH 7.5, 0.5 M NaCl, 1% Triton X-100, 0.5 M urea) for 10 min (RPE1 cells) to 17 min (DLD1 CENP-A^{AID} cells) and slowly removed from lysis buffer to stretch DNA into long fibers. Fibers were fixed in 4% PFA and permeabilized in KCM. Slides were then subjected to CENP-A immunostaining and FISH to detect the X alpha-satellite array DXZ1. CENP-A antibody (ab13939; Abcam) concentration was increased to 1:75 and DXZ1 HOR DNA FISH probe (pBAMX7B) amount used at a concentration of ~500 ng per 22 × 40 mm slide area.

All images were acquired using an inverted Olympus IX-71 microscope controlled by the Deltavision Elite Imaging System (Applied Precision) equipped with a Photometric CoolSNAP HQ^2 CCD camera. Fiber images were collected using the 100× objective. Fibers extending through multiple fields of view were captured using the Panels option in the softWoRx Acquire 3D program and merged into single images using the "Stitch" function. All images were exported for analysis and visualization into Adobe Photoshop and ImageJ.

The "Measure Distances" tool of SoftWorx was used to calculate lengths of fluorescent signals representing euchromatic probe, alpha-satellite probes, or CENP-A immunostaining as previously described (Sullivan *et al*, 2011). CENP-A domain size was measured by comparing the length of CENP-A antibody staining (in micrometers) to the length of overlapping DXZ1 alpha-satellite FISH probe (pBAMX7B). Alpha-satellite FISH probe signal length represented total satellite array size that had been determined by pulsed-field gel electrophoresis. CENP-A chromatin domain size was calculated from the ratio of the length of CENP-A antibody signal over the total length of alpha-satellite FISH signal.

Intensity quantifications in microscopy experiments

We quantified signal intensities of centromeres on interphase cells manually or automatically as described previously (Fachinetti *et al*, 2013, 2015). Integrated densities were determined using the software FIJI. In the case of manual quantification, a 15 × 15-pixel circle was drawn around the centromere (marked by CENP-B or CENP-B box staining), and an identical circle was drawn nearby (background). The integrated intensity of each centromere was calculated by subtracting the background signal from the centromeric signal. 15 centromeres per cell were averaged to determine the average centromere intensity for each cell. The same quantifications were performed using a 30 × 30-pixel circle to determine CENP-C and CENP-A intensities at the LacO array avoiding inclusion of adjacent native centromeres.

To quantify total nuclear signal, the nuclear area was identified via the DAPI staining. The nuclear-integrated intensity of EYFP signal was calculated by subtracting the background signal measured outside the DAPI signal. To calculate the difference in signal intensity between nuclear and centromeric CENP-A, the integrated intensity of EYFP at centromeres was quantified as described above, but the background was also taken outside the DAPI signal. The sum of the measurements of all centromeres was then taken into consideration and subtracted from the total nuclear signal.

Cloning, expression, and protein purification

pET30-His-CENP-B (161–599) and His-CENP-B (161–404; 465–599) generated using the Gibson Assembly® kit (Neb) were used for protein expression in bacteria, and pFB-GST-CENP-C (1-727) was used for protein expression in Sf9 cells as described previously (Fachinetti *et al*, 2015). CENP-B constructs were expressed in BL21 pLysS (Agilent) at 37°C in 2-YT medium supplemented with Kanamycin (50 μg/ml) and chloramphenicol (35 μg/ml) until $OD_{600\ nm}$ between 0.6 and 0.8. Recombinant protein expression was induced by addition of 0.5 mM IPTG (isopropyl β-D-1-thiogalactopyranoside). Cell cultures were incubated overnight at 20°C and then harvested by centrifugation 4,500 *g* 30 min. Cell culture pellets from bacteria or insect cells were suspended in Buffer A (His-CENP-B constructs: 20 mM Tris pH 8, 200 mM NaCl, 2 mM β-mercaptoethanol, protease inhibitor (Roche), 1 mM phenylmethylsulfonyl fluoride (PMSF), 20 mM Imidazole pH 8, GST-CENP-C: 20 mM HEPES pH 7.5, 500 mM NaCl, 1 mM DTT, 1 mM PMSF, protease inhibitor (Roche), 0,1% Triton X-100). His-CENP-B constructs from bacteria and CENP-C Sf9 cells were lysed respectively by sonication or cell homogenizer, then centrifuged for 30 min at 45,000 *g*. The clear lysate was loaded onto a 5 ml GST-Trap (GE Healthcare) for GST-CENP-C or a 5 ml His-Trap crude FF (GE Healthcare) for His tagged CENP-B variants connected to an Äkta Pure (GE Healthcare). Nonspecific proteins were removed by washing the column with buffer A, the proteins of interest were eluted with a linear gradient Buffer B (His-CENP-B constructs: 20 mM Tris pH 8, 200 mM NaCl, 2 mM β-mercaptoethanol, 1 mM phenylmethylsulfonyl fluoride (PMSF), 350 mM Imidazole pH 8; GST-CENP-C: 20 mM HEPES pH 7.5, 500 mM NaCl, 1 mM DTT, 1 mM PMSF, 20 mM reduced glutathione pH 7.5). For His-CENP-B (161-599), an anion exchange chromatography was performed subsequently. The protein of interest was loaded onto a capto Q impress 1 mL (GE Healthcare) connected to an Äkta Pure (GE Healthcare). Nonspecific proteins were removed by washing the column with buffer C (20 mM Tris pH 8, 200 mM NaCl, 1 mM DTT), the proteins of interest were eluted with a linear gradient Buffer D (20 mM Tris pH8, 1M NaCl, 1 mM DTT). Size exclusion chromatography was then performed for all constructs on the fractions containing eluted proteins using buffer E (His-CENP-B constructs: 20 mM Tris pH 8, 200 mM NaCl, 1 mM DTT; GST-CENP-C: 20 mM HEPES pH 7.5, 500 mM NaCl, 1 mM DTT, 1 mM PMSF) on a Superdex 200 column connected to an Äkta Pure (GE Healthcare).

GST pull-down assay

100 μl of glutathione sepharose beads 50% (GE healthcare) was washed 4 times with 1,000 μl of interaction Buffer (20 mM HEPES pH 7.5, 300 mM KCl, 1 mM DTT, 5% glycerol). Recombinant His-CENP-B variants and/or GST-CENP-C were added at a final concentration of 2 μM in 100 μl then incubated for 1 h at RT. Beads were then washed 3 times with 1000 μl of buffer A then 1 time with 1000 μl of PBS. Proteins are finally eluted with 50 μl of elution buffer (20 mM HEPES pH 7.5, 500 mM NaCl, 1 mM DTT, 5% glycerol, 20 mM reduced glutathione). 25 μl of SB5X is added to 25 μl of INPUT and elution, and boiled 5 min at 95°C; then, 12 μl is loaded on mini protein precast gels (Bio-Rad). The presence of the proteins was revealed by immunoblot.

$CD4^+$ T-cell staining and sorting

Peripheral blood mononuclear cells (PBMCs) were isolated from platelet apheresis blood from healthy human donors (approved by the Institut National de la Santé et de la Recherche Médicale committee) using Ficoll-Paque PLUS (GE Healthcare). Total $CD4^+$ T-cell enrichment was performed by negative selection with an EasySep Human $CD4^+$ T-cell Isolation Kit (Stem Cell Technologies, ref. 17952).

Cell surface staining to assess $CD4^+$ T-cell enrichment

Staining was performed in FACS buffer: 1% BSA (Sigma, ref. A7030-10G) and 1 mM EDTA (Thermo Fisher, ref. 15575020) in PBS. Antibodies used were as follows: anti-human CD14 (clone M5E2, BD Biosciences, cat. 560919) and anti-human CD4 (clone RPA-T4, BD Biosciences, cat. 557871). Cells were stained for 15 min at 4°C and washed twice. Data were acquired on a FACSVerse flow cytometer (BD) and analyzed in FlowJo (TreeStar). $CD4^+$ T-cell enrichment was always superior to 95%.

Intracellular staining of CENP-A & CENP-B, and cell sorting

Freshly purified $CD4^+$ T cells were washed once with PBS and stained with Fixable Viability dye eFluor 780 (eBiosciences, ref. 65-0865-14) for 30 min at 4°C in PBS. Cells were washed twice in PBS, fixed and permeabiized using FoxP3 Staining buffer set (Thermo Fisher, ref. 00-5523-00) according to the manufacturer's instructions. Intracellular staining was performed in permeabilization buffer using mouse anti-human CENP-A (clone 3-19, ENZO, ref. ADI-KAM-CC006-E) and rabbit anti-human CENP-B (Abcam, ref. ab25734). Mouse IgG1 kappa (eBiosciences, ref. 14-4714-82) and rabbit IgG (Thermo Fisher, ref. 10500C) were used as isotype controls. Cells were washed twice with permeabilization buffer and stained with secondary antibodies: F(ab')2-Goat anti-mouse IgG (H+L) (Thermo Fisher, ref. A-11017) and goat anti-rabbit IgG (H+L) antibody (Thermo Fisher, ref. A-21245). Each staining was performed for 30 min at 4°C. Cells were washed twice with permeabilization buffer and resuspended in FACS buffer for FACS acquisition or cell sorting. Dead cells were gated as eFluor780+, and CENP-A and CENP-B expression was assessed in alive cells, and gated as $eFluor780^-$. Cell sorting was performed on a MoFlo Astrios (Beckman Coulter). Sorted populations purity was superior to 98%.

To track cell division, purified $CD4^+$ T cells were labeled with carboxyfluorescein succinimidyl ester (CFSE, eBioscience, ref. 850850-84). Cells were washed once in PBS and stained with 1.6°μM CFSE in PBS at a concentration of 10 millions cells per ml. Cells were incubated at 37°C for 3 min in the dark, and staining was

stopped by adding cold 50% serum in PBS and letting cells on ice for 3 min in the dark. Cells were centrifuged and washed with cold 50% serum and X-VIVO15 medium (Lonza, ref. BE02-060F). Cells were then plated onto 12-well plates at 1 million per ml in X-VIVO15 containing penicillin/streptomycin (Invitrogen) and 100 U/ml IL-2 (ImmunoTools, ref. 11340027). Cells were activated with Dynabeads Human T-Activator CD3/CD28 (Thermo Fisher, ref. 11131D) and incubated at 37°C for 5 days. Cells were counted every day with LUNA automated cell counter (Logos biosystems). At day 3 post-activation, media was changed and cells were plated at 1 million per ml.

Sorted CENP-A-high and low expressing cells were cytospin using a Shandon Cytospin 4 (Thermo Fisher) onto coverglasses at 250 *g* for 5 min. Cells were fixed with 4% Formaldehyde for 5 min at room temperature, DAPI counterstained, and mounted using anti-fading mounting reagent (Life Technologies).

Data availability

Sequencing data for the CENP-A CUT&RUN on non-treated and IAA wash-out samples, with corresponding negative controls, are available at GEO (https://www.ncbi.nlm.nih.gov/geo/) under the accession numbers GSM3852804, GSE148187, GSM3852807, and GSM3852808, respectively.

Expanded View for this article is available online.

Acknowledgements
The authors would like to thank (from I. Curie, FR): C. Bartocci, A. Coulon, P. Tran, the Basto and Drinnenberg team members, A. Scelfo, S. Gangnard, and all other Fachinetti team members for helpful suggestions and G. Bersano-Marchisio for cell line generation. We would also like to thank S. Marcand (CEA, FR), B. Black and G. Logsdon (UPENN, USA), I. Cheeseman (MIT, USA), D. Cleveland and A. Desai (UCSD, USA) P. Maddox (UNC, USA), D. Foltz (Northwestern University, USA), L. Jansen (University of Oxford, UK), A. Straight (Stanford, USA), W. Earnshaw (Wellcome Centre, UK) and G. Almouzni and F. Perez (I. Curie, FR) for helpful suggestions and/or providing reagents. We also would like to thank A. Houdusse and C. Kikuti (I. Curie, FR) for technical suggestions and the usage of biochemical equipment. We also thank the flow cytometry platform, the Cell and Tissue Imaging facility (PICT-IBiSA, member of the French National Research Infrastructure France-BioImaging ANR10-INBS-04), the antibody facility platform, and the sequencing platform at Institut Curie. S.M.M was supported by National Science Foundation Graduate Research Fellowship DGE-1644868, and B.A.S. received research support from National Institutes of Health grant R01 GM124041. R.G. is supported by AIRC post-doctoral fellowship for abroad and H.M.I. by I. Curie and a Séneca post-doctoral fellowship ref. 20941/PD/18. N.M. received support from LABEX DCBIOL, ANR (ANR-17-CE15-0025-01, ANR-18-CE92-0022-01, ANR-19-CE15-0018-01), INSERM (19CS007-00), ANRS. D.F. receives salary support from the CNRS. D.F. has received support for this project by Labex « Cell(n)Scale », the Institut Curie, the ATIP-Avenir ITMO Cancer 2015 program, the program «Investissements d'Avenir» launched by the French Government and implemented by ANR with the references ANR-10-LABX-0038 and ANR-10-IDEX-0001-02 PSL and the Emergence grant 2018 from the city of Paris. S.H. received funding from the European Union's Horizon 2020 research and innovation program under the Marie Skłodowska-Curie grant agreement No 666003 and the French foundation for medical research (FRM, FDT201904008185).

Author contributions
HMI conceived and performed the experiments on $CD4^+$ T cells under the supervision of NM; RG performed all chromatin–protein interaction experiments and bioinformatic analysis. FC performed *in vitro* protein purification and interaction; MD performed and analyzed some of LacO/I experiments and helped in other assays. VK performed and analyzed single molecule experiments; SMM performed and analyzed the chromatin fiber and metaphase chromosome line scan experiments under the supervision of BAS; SHe helped with image analysis. SHo performed and analyzed all other experiments. DF and SHo conceived the experimental design, made figures, and wrote the manuscript. DF directed the research. All authors contributed to manuscript editing.

Conflict of interest
The authors declare that they have no conflict of interest.

References

Allshire RC, Karpen GH (2008) Epigenetic regulation of centromeric chromatin: old dogs, new tricks? *Nat Rev Genet* 9: nrg2466–937

Amor DJ, Bentley K, Ryan J, Perry J, Slater H, Choo KHA (2004) Human centromere repositioning "in progress". *Proc Natl Acad Sci USA* 101: 6542 – 6547

Aze A, Sannino V, Soffientini P, Bachi A, Costanzo V (2016) Centromeric DNA replication reconstitution reveals DNA loops and ATR checkpoint suppression. *Nat Cell Biol* 18: 684 – 691

Bailey AO, Panchenko T, Shabanowitz J, Lehman SM, Bai DL, Hunt DF, Black BE, Foltz DR (2016) Identification of the post-translational modifications present in centromeric chromatin. *Mol Cell Proteomics* 15: 918 – 931

Barnhart MC, Kuich PHJL, Stellfox ME, Ward JA, Bassett EA, Black BE, Foltz DR (2011) HJURP is a CENP-A chromatin assembly factor sufficient to form a functional *de novo* kinetochore. *J Cell Biol* 194: 229 – 243

Barra V, Fachinetti D (2018) The dark side of centromeres: types, causes and consequences of structural abnormalities implicating centromeric DNA. *Nat Commun* 9: 4340

Barra V, Logsdon GA, Scelfo A, Hoffmann S, Hervé S, Aslanian A, Nechemia-Arbely Y, Cleveland DW, Black BE, Fachinetti D (2019) Phosphorylation of CENP-A on serine 7 does not control centromere function. *Nat Commun* 10: 1 – 10

Bassett EA, DeNizio J, Barnhart-Dailey MC, Panchenko T, Sekulic N, Rogers DJ, Foltz DR, Ben Black E (2012) HJURP uses distinct CENP-A surfaces to recognize and to stabilize CENP-A/Histone H4 for centromere assembly. *Dev Cell* 22: 749 – 762

Bergmann JH, Gómez Rodríguez M, Martins NMC, Kimura H, Kelly DA, Masumoto H, Larionov V, Jansen LET, Earnshaw WC (2010) Epigenetic engineering shows H3K4me2 is required for HJURP targeting and CENP-A assembly on a synthetic human kinetochore. *EMBO J* 30: 328 – 340

Bernad R, Sánchez P, Rivera T, Rodríguez-Corsino M, Boyarchuk E, Vassias I, Ray-Gallet D, Arnaoutov A, Dasso M, Almouzni G *et al* (2011) Xenopus HJURP and condensin II are required for CENP-A assembly. *J Cell Biol* 192: 569 – 582

Black BE, Foltz DR, Chakravarthy S, Luger K, Woods VL, Cleveland DW (2004) Structural determinants for generating centromeric chromatin. *Nature* 430: 578 – 582

Black BE, Brock MA, Bédard S, Woods VL, Cleveland DW (2007) An epigenetic mark generated by the incorporation of CENP-A into centromeric nucleosomes. *Proc Natl Acad Sci USA* 104: 5008 – 5013

Bobkov GOM, Gilbert N, Heun P (2018) Centromere transcription allows CENP-A to transit from chromatin association to stable incorporation. *J Cell Biol* 217: 1957 – 1972

Bodor DL, Mata JF, Sergeev M, David AF, Salimian KJ, Panchenko T, Cleveland DW, Black BE, Shah JV, Jansen LE (2014) The quantitative architecture of centromeric chromatin. *Elife* 3: e02137

Carroll CW, Silva MCC, Godek KM, Jansen LET, Straight AF (2009) Centromere assembly requires the direct recognition of CENP-A nucleosomes by CENP-N. *Nat Cell Biol* 11: 896 – 902

Carroll CW, Milks KJ, Straight AF (2010) Dual recognition of CENP-A nucleosomes is required for centromere assembly. *J Cell Biol* 189: 1143 – 1155

Chan FL, Marshall OJ, Saffery R, Kim BW, Earle E, Choo KHA, Wong LH (2012) Active transcription and essential role of RNA polymerase II at the centromere during mitosis. *Proc Natl Acad Sci USA* 109: 1979 – 1984

Chen C-C, Bowers S, Lipinszki Z, Palladino J, Trusiak S, Bettini E, Rosin L, Przewloka MR, Glover DM, O'Neill RJ *et al* (2015) Establishment of centromeric chromatin by the CENP-A assembly factor CAL1 requires FACT-mediated transcription. *Dev Cell* 34: 73 – 84

Contreras-Galindo R, Fischer S, Saha AK, Lundy JD, Cervantes PW, Mourad M, Wang C, Qian B, Dai M, Meng F, *et al* (2017) Rapid molecular assays to study human centromere genomics. *Genome Res* 27: 2040 – 2049

Dambacher S, Deng W, Hahn M, Sadic D, Fröhlich J, Nuber A, Hoischen C, Diekmann S, Leonhardt H, Schotta G (2012) CENP-C facilitates the recruitment of M18BP1 to centromeric chromatin. *Nucleus* 3: 101 – 110

Dumont M, Gamba R, Gestraud P, Klaasen S, Worrall JT, De Vries SG, Boudreau V, Luypaert CS, Maddox PS, Lens SM *et al* (2020) Human chromosome-specific aneuploidy is influenced by DNA-dependent centromeric features. *EMBO J* 39: 1132 – 1130

Dunleavy EM, Roche D, Tagami H, Lacoste N, Ray-Gallet D, Nakamura Y, Daigo Y, Nakatani Y, Almouzni-Pettinotti G (2009) HJURP is a cell-cycle-dependent maintenance and deposition factor of CENP-A at centromeres. *Cell* 137: 485 – 497

Earnshaw WC, Rothfield N (1985) Identification of a family of human centromere proteins using autoimmune sera from patients with scleroderma. *Chromosoma* 91: 313 – 321

Earnshaw WC, Ratrie H, Stetten G (1989) Visualization of centromere proteins CENP-B and CENP-C on a stable dicentric chromosome in cytological spreads. *Chromosoma* 98: 1 – 12

Fachinetti D, Folco HD, Nechemia-Arbely Y, Valente LP, Nguyen K, Wong AJ, Zhu Q, Holland AJ, Desai A, Jansen LET *et al* (2013) A two-step mechanism for epigenetic specification of centromere identity and function. *Nat Cell Biol* 15: 1056 – 1066

Fachinetti D, Han JS, McMahon MA, Ly P, Abdullah A, Wong AJ, Cleveland DW (2015) DNA sequence-specific binding of CENP-B enhances the fidelity of human centromere function. *Dev Cell* 33: 314 – 327

Falk SJ, Guo LY, Sekulic N, Smoak EM, Mani T, Logsdon GA, Gupta K, Jansen LET, Van Duyne GD, Vinogradov SA *et al* (2015) Chromosomes. CENP-C reshapes and stabilizes CENP-A nucleosomes at the centromere. *Science* 348: 699 – 703

Falk SJ, Lee J, Sekulic N, Sennett MA, Lee T-H, Black BE (2016) CENP-C directs a structural transition of CENP-A nucleosomes mainly through sliding of DNA gyres. *Nature* 23: 204 – 208

Foltz DR, Jansen LET, Black BE, Bailey AO, Yates JR, Cleveland DW (2006) The human CENP-A centromeric nucleosome-associated complex. *Nat Cell Biol* 8: 458 – 469

Foltz DR, Jansen LET, Bailey AO, Yates JR III, Bassett EA, Wood S, Black Ben E, Cleveland DW (2009) Centromere-specific assembly of CENP-A nucleosomes is mediated by HJURP. *Cell* 137: 472 – 484

French BT, Westhorpe FG, Limouse C, Straight AF (2017) Xenopus laevis M18BP1 Directly Binds Existing CENP-A Nucleosomes to Promote Centromeric Chromatin Assembly. *Dev Cell* 42: 190 – 199.e10

Fujita R, Otake K, Arimura Y, Horikoshi N, Miya Y, Shiga T, Osakabe A, Tachiwana H, Ohzeki J-I, Larionov V *et al* (2015) Stable complex formation of CENP-B with the CENP-A nucleosome. *Nucleic Acids Res* 43: 4909 – 4922

Fukagawa T, Earnshaw WC (2014) The centromere: chromatin foundation for the kinetochore machinery. *Dev Cell* 30: 496 – 508

Gamba R, Fachinetti D (2020) From evolution to function: two sides of the same CENP-B coin? *Exp Cell Res* 390: 111959

Gascoigne KE, Takeuchi K, Suzuki A, Hori T, Fukagawa T, Cheeseman IM (2011) Induced ectopic kinetochore assembly bypasses the requirement for CENP-A nucleosomes. *Cell* 145: 410 – 422

Gassmann R, Rechtsteiner A, Yuen KW, Muroyama A, Egelhofer T, Gaydos L, Barron F, Maddox P, Essex A, Monen J *et al* (2012) An inverse relationship to germline transcription defines centromeric chromatin in *C. elegans*. *Nature* 484: 534 – 537

Guse A, Carroll CW, Moree B, Fuller CJ, Straight AF (2011) *In vitro* centromere and kinetochore assembly on defined chromatin templates. *Nature* 477: 354 – 358

Harkes R, Keizer VIP, Schaaf MJM, Schmidt T (2015) Depth-of-focus correction in single-molecule data allows analysis of 3D diffusion of the glucocorticoid receptor in the nucleus. *PLoS ONE* 10: e0141080

Heun P, Erhardt S, Blower MD, Weiss S, Skora AD, Karpen GH (2006) Mislocalization of the *Drosophila* centromere-specific histone CID promotes formation of functional ectopic kinetochores. *Dev Cell* 10: 303 – 315

Hochegger H, Dejsuphong D, Sonoda E, Saberi A, Rajendra E, Kirk J, Hunt T, Takeda S (2007) An essential role for Cdk1 in S phase control is revealed via chemical genetics in vertebrate cells. *J Cell Biol* 178: 257 – 268

Hoffmann S, Dumont M, Barra V, Ly P, Nechemia-Arbely Y, McMahon MA, Hervé S, Cleveland DW, Fachinetti D (2016) CENP-A is dispensable for mitotic centromere function after initial centromere/kinetochore assembly. *Cell Rep* 17: 2394 – 2404

Hoffmann S, Fachinetti D (2018) Real-time *de novo* deposition of centromeric histone-associated proteins using the auxin-inducible degradation system. *Methods Mol Biol* 1832: 223 – 241

Holland AJ, Fachinetti D, Han JS, Cleveland DW (2012) Inducible, reversible system for the rapid and complete degradation of proteins in mammalian cells. *Proc Natl Acad Sci USA* 109: E3350 – E3357

Hori T, Amano M, Suzuki A, Backer CB, Welburn JP, Dong Y, McEwen BF, Shang W-H, Suzuki E, Okawa K *et al* (2008) CCAN makes multiple contacts with centromeric DNA to provide distinct pathways to the outer kinetochore. *Cell* 135: 1039 – 1052

Hori T, Shang W-H, Takeuchi K, Fukagawa T (2013) The CCAN recruits CENP-A to the centromere and forms the structural core for kinetochore assembly. *J Cell Biol* 200: 45 – 60

Hori T, Shang W-H, Hara M, Ariyoshi M, Arimura Y, Fujita R, Kurumizaka H, Fukagawa T (2017) Association of M18BP1/KNL2 with CENP-A nucleosome is essential for centromere formation in non-mammalian vertebrates. *Dev Cell* 42: 181 – 189.e3

Hudson DF, Fowler KJ, Earle E, Saffery R, Kalitsis P, Trowell H, Hill J, Wreford NG, de Kretser DM, Cancilla MR *et al* (1998) Centromere protein B null mice are mitotically and meiotically normal but have lower body and testis weights. *J Cell Biol* 141: 309 – 319

Iwamoto M, Björklund T, Lundberg C, Kirik D, Wandless TJ (2010) A general chemical method to regulate protein stability in the mammalian central nervous system. *Chem Biol* 17: 981 – 988

Janicki SM, Tsukamoto T, Salghetti SE, Tansey WP, Sachidanandam R, Prasanth KV, Ried T, Shav-Tal Y, Bertrand E, Singer RH *et al* (2004) From silencing to gene expression: real-time analysis in single cells. *Cell* 116: 683 – 698

Jansen LET, Black BE, Foltz DR, Cleveland DW (2007) Propagation of centromeric chromatin requires exit from mitosis. *J Cell Biol* 176: 795 – 805

Kapoor M, de Oca Luna RM, Liu G, Lozano G, Cummings C, Mancini M, Ouspenski I, Brinkley BR, May GS (1998) The cenpB gene is not essential in mice. *Chromosoma* 107: 570 – 576

Karolchik D, Hinrichs AS, Furey TS, Roskin KM, Sugnet CW, Haussler D, Kent WJ (2004) The UCSC table browser data retrieval tool. *Nucleic Acids Res* 32: D493 – D496

Kasinathan S, Henikoff S (2018) Non-B-form DNA is enriched at centromeres. *Mol Biol Evol* 26: 1301 – 1314

Kato H, Jiang J, Zhou BR, Rozendaal M, Feng H, Ghirlando R, Xiao TS, Straight AF, Bai Y (2013) A conserved mechanism for centromeric nucleosome recognition by centromere protein CENP-C. *Science* 340: 1110 – 1113

Klare K, Weir JR, Basilico F, Zimniak T, Massimiliano L, Ludwigs N, Herzog F, Musacchio A (2015) CENP-C is a blueprint for constitutive centromere–associated network assembly within human kinetochores. *J Cell Biol* 210: 11 – 22

Kyriacou E, Heun P (2018) High-resolution mapping of centromeric protein association using APEX-chromatin fibers. *Epigenet Chrom* 11: 68 – 17

Lacoste N, Woolfe A, Tachiwana H, Garea AV, Barth T, Cantaloube S, Kurumizaka H, Imhof A, Almouzni G (2014) Mislocalization of the centromeric histone variant CenH3/CENP-A in human cells depends on the chaperone DAXX. *Mol Cell* 53: 631 – 644

Li H, Durbin R (2009) Fast and accurate short read alignment with Burrows-Wheeler transform. *Bioinformatics* 25: 1754 – 1760

Li H (2013) Aligning sequence reads, clone sequences and assembly contigs with BWA-MEM. arXiv: 1303.3997 [q-bio.GN] [PREPRINT]

Logsdon GA, Gambogi CW, Liskovykh MA, Barrey EJ, Larionov V, Miga KH, Heun P, Black BE (2019) Human artificial chromosomes that bypass centromeric DNA. *Cell* 178: 624 – 639.e19

Lou X, Hou Y, Liang D, Peng L, Chen H, Ma S, Zhang L (2015) A novel Alu-based real-time PCR method for the quantitative detection of plasma circulating cell-free DNA: sensitivity and specificity for the diagnosis of myocardial infarction. *Int J Mol Med* 35: 72 – 80

Ly P, Teitz LS, Kim DH, Shoshani O, Skaletsky H, Fachinetti D, Page DC, Cleveland DW (2017) Selective Y centromere inactivation triggers chromosome shattering in micronuclei and repair by non-homologous end joining. *Nat Cell Biol* 19: 68 – 75

Maloney KA, Sullivan LL, Matheny JE, Strome ED, Merrett SL, Ferris A, Sullivan BA (2012) Functional epialleles at an endogenous human centromere. *Proc Natl Acad Sci USA* 109: 13704 – 13709

Marshall OJ, Chueh AC, Wong LH, Choo KHA (2008) Neocentromeres: new insights into centromere structure. *Dis Dev Karyotype Evol* 82: 261 – 282

McKinley KL, Cheeseman IM (2014) Polo-like kinase 1 licenses CENP-A deposition at centromeres. *Cell* 158: 397 – 411

McKinley KL, Sekulic N, Guo LY, Tsinman T, Black BE, Cheeseman IM (2015) The CENP-L-N complex forms a critical node in an integrated meshwork of interactions at the centromere-kinetochore interface. *Mol Cell* 60: 886 – 898

McKinley KL, Cheeseman IM (2016) The molecular basis for centromere identity and function. *Nat Rev Mol Cell Biol* 17: 16 – 29

McNulty SM, Sullivan LL, Sullivan BA (2017) Human centromeres produce chromosome-specific and array-specific alpha satellite transcripts that are complexed with CENP-A and CENP-C. *Dev Cell* 42: 226 – 240.e6

Miga KH, Newton Y, Jain M, Altemose N, Willard HF, Kent WJ (2014) Centromere reference models for human chromosomes X and Y satellite arrays. *Genome Res* 24: 697 – 707

Miga KH (2017) The promises and challenges of genomic studies of human centromeres. *Prog Mol Subcell Biol* 56: 285 – 304

Moree B, Meyer CB, Fuller CJ, Straight AF (2011) CENP-C recruits M18BP1 to centromeres to promote CENP-A chromatin assembly. *J Cell Biol* 194: 855 – 871

Morozov VM, Giovinazzi S, Ishov AM (2017) CENP-B protects centromere chromatin integrity by facilitating histone deposition via the H3.3-specific chaperone Daxx. *Epigenet Chrom* 10: 63

Müller S, Montes de Oca R, Lacoste N, Dingli F, Loew D, Almouzni G (2014) Phosphorylation and DNA binding of HJURP determine its centromeric recruitment and function in CenH3(CENP-A) loading. *Cell Rep* 8: 190 – 203

Musacchio A, Desai A (2017) A molecular view of kinetochore assembly and function. *Biology* 6: 5

Nardi IK, Zasadzińska E, Stellfox ME, Knippler CM, Foltz DR (2016) Licensing of centromeric chromatin assembly through the Mis18α-Mis18β heterotetramer. *Mol Cell* 61: 774 – 787

Nechemia-Arbely Y, Fachinetti D, Miga KH, Sekulic N, Soni GV, Kim DH, Wong AK, Lee AY, Nguyen K, Dekker C *et al* (2017) Human centromeric CENP-A chromatin is a homotypic, octameric nucleosome at all cell cycle points. *J Cell Biol* 216: 607 – 621

Nechemia-Arbely Y, Miga KH, Shoshani O, Aslanian A, McMahon MA, Lee AY, Fachinetti D, Yates JR, Ren B, Cleveland DW (2019) DNA replication acts as an error correction mechanism to maintain centromere identity by restricting CENP-A to centromeres. *Nat Cell Biol* 21: 743 – 754

Niikura Y, Kitagawa R, Ogi H, Abdulle R, Pagala V, Kitagawa K (2015) CENP-A K124 ubiquitylation is required for CENP-A deposition at the centromere. *Dev Cell* 32: 589 – 603

Niikura Y, Kitagawa R, Kitagawa K (2016) CENP-A ubiquitylation is inherited through dimerization between cell divisions. *Cell Rep* 15: 61 – 76

Nishimura K, Fukagawa T, Takisawa H, Kakimoto T, Kanemaki M (2009) An auxin-based degron system for the rapid depletion of proteins in nonplant cells. *Nat Methods* 6: 917 – 922

Ohzeki JI, Nakano M, Okada T, Masumoto H (2002) CENP-B box is required for *de novo* centromere chromatin assembly on human alphoid DNA. *J Cell Biol* 159: 765 – 775

Ohzeki JI, Shono N, Otake K, Martins NMC, Kugou K, Kimura H, Nagase T, Larionov V, Earnshaw WC, Masumoto H (2016) KAT7/HBO1/MYST2 regulates CENP-A chromatin assembly by antagonizing Suv39h1-mediated centromere inactivation. *Dev Cell* 37: 413 – 427

Ohzeki JI, Larionov V, Earnshaw WC, Masumoto H (2019) *De novo* formation and epigenetic maintenance of centromere chromatin. *Curr Opin Cell Biol* 58: 15 – 25

Okada M, Cheeseman IM, Hori T, Okawa K, McLeod IX, Yates JR, Desai A, Fukagawa T (2006) The CENP-H-I complex is required for the efficient incorporation of newly synthesized CENP-A into centromeres. *Nat Cell Biol* 8: 446 – 457

Okada T, Ohzeki J-I, Nakano M, Yoda K, Brinkley WR, Larionov V, Masumoto H (2007) CENP-B controls centromere formation depending on the chromatin context. *Cell* 131: 1287 – 1300

Olszak AM, van Essen D, Pereira AJ, Diehl S, Manke T, Maiato H, Saccani S, Heun P (2011) Heterochromatin boundaries are hotspots for *de novo* kinetochore formation. *Nature* 13: 799 – 808

Otake K, Ohzeki J-I, Shono N, Kugou K, Okazaki K, Nagase T, Yamakawa H, Kouprina N, Larionov V, Kimura H *et al* (2020) CENP-B creates alternative epigenetic chromatin states permissive for CENP-A or heterochromatin assembly. *J Cell Sci* 133: jcs243303

Palmer DK, O'Day K, Wener MH, Andrews BS, Margolis RL (1987) A 17-kD centromere protein (CENP-A) copurifies with nucleosome core particles and with histones. *J Cell Biol* 104: 805 – 815

Pan D, Klare K, Petrovic A, Take A, Walstein K, Singh P, Rondelet A, Bird AW, Musacchio A (2017) CDK-regulated dimerization of M18BP1 on a Mis18 hexamer is necessary for CENP-A loading. *Elife* 6: e23352

Pan D, Walstein K, Take A, Bier D, Kaiser N, Musacchio A (2019) Mechanism of centromere recruitment of the CENP-A chaperone HJURP and its implications for centromere licensing. *Nat Commun* 10: 4046

Perez-Castro AV, Shamanski FL, Meneses JJ, Lovato TL, Vogel KG, Moyzis RK, Pedersen R (1998) Centromeric protein B null mice are viable with no apparent abnormalities. *Dev Biol* 201: 135 – 143

Pesenti ME, Prumbaum D, Auckland P, Smith CM, Faesen AC, Petrovic A, Erent M, Maffini S, Pentakota S, Weir JR *et al* (2018) Reconstitution of a 26-subunit human kinetochore reveals cooperative microtubule binding by CENP- OPQUR and NDC80. *Mol Cell* 71: 923 – 939.e10

Politi V, Perini G, Trazzi S, Pliss A, Raska I, Earnshaw WC, Valle Della G (2002) CENP-C binds the alpha-satellite DNA *in vivo* at specific centromere domains. *J Cell Sci* 115: 2317 – 2327

Quénet D, Dalal Y, Shilatifard A (2014) A long non-coding RNA is required for targeting centromeric protein A to the human centromere. *Elife* 3: e03254-218

Ramírez F, Ryan DP, Grüning B, Bhardwaj V, Kilpert F, Richter AS, Heyne S, Dündar F, Manke T (2016) deepTools2: a next generation web server for deep-sequencing data analysis. *Nucleic Acids Res* 44: W160 – W165

Ross JE, Woodlief KS, Sullivan BA (2016) Inheritance of the CENP-A chromatin domain is spatially and temporally constrained at human centromeres. *Epigenet Chrom* 9: 20 – 18

Saldivar JC, Hamperl S, Bocek MJ, Chung M, Bass TE, Cisneros-Soberanis F, Samejima K, Xie L, Paulson JR, Earnshaw WC *et al* (2018) An intrinsic S/G2 checkpoint enforced by ATR. *Science* 361: 806 – 810

Santaguida S, Musacchio A (2009) The life and miracles of kinetochores. *EMBO J* 28: 2511 – 2531

Scelfo A, Fachinetti D (2019) Keeping the centromere under control: a promising role for DNA methylation. *Cells* 8: 912

Schneider VA, Graves-Lindsay T, Howe K, Bouk N, Chen H-C, Kitts PA, Murphy TD, Pruitt KD, Thibaud-Nissen F, Albracht D *et al* (2017) Evaluation of GRCh38 and *de novo* haploid genome assemblies demonstrates the enduring quality of the reference assembly. *Genome Res* 27: 849 – 864

Shang W-H, Hori T, Martins NMC, Toyoda A, Misu S, Monma N, Hiratani I, Maeshima K, Ikeo K, Fujiyama A *et al* (2013) Chromosome engineering allows the efficient isolation of vertebrate neocentromeres. *Dev Cell* 24: 635 – 648

Shang W-H, Hori T, Westhorpe FG, Godek KM, Toyoda A, Misu S, Monma N, Ikeo K, Carroll CW, Takami Y *et al* (2016) Acetylation of histone H4 lysine 5 and 12 is required for CENP-A deposition into centromeres. *Nat Commun* 7: 13465 – 13

Shelby RD, Vafa O, Sullivan KF (1997) Assembly of CENP-A into centromeric chromatin requires a cooperative array of nucleosomal DNA contact sites. *J Cell Biol* 136: 501 – 513

Shono N, Ohzeki J-I, Otake K, Martins NMC, Nagase T, Kimura H, Larionov V, Earnshaw WC, Masumoto H (2015) CENP-C and CENP-I are key connecting factors for kinetochore and CENP-A assembly. *J Cell Sci* 128: 4572 – 4587

Shukla M, Tong P, White SA, Singh PP, Reid AM, Catania S, Pidoux AL, Allshire RC (2018) Centromere DNA destabilizes H3 nucleosomes to promote CENP-A deposition during the cell cycle. *Curr Biol* 28: 3924 – 3936.e4

Silva MCC, Bodor DL, Stellfox ME, Martins NMC, Hochegger H, Foltz DR, Jansen LET (2012) Cdk activity couples epigenetic centromere inheritance to cell cycle progression. *Dev Cell* 22: 52 – 63

Skene PJ, Henikoff S (2017) An efficient targeted nuclease strategy for high-resolution mapping of DNA binding sites. *Elife* 6: 576

Stankovic A, Guo LY, Mata JF, Bodor DL, Cao X-J, Bailey AO, Shabanowitz J, Hunt DF, Garcia BA, Black BE *et al* (2016) A dual inhibitory mechanism sufficient to maintain cell-cycle-restricted CENP-A assembly. *Mol Cell* 65: 231 – 246

Stankovic A, Jansen LET (2017) Quantitative microscopy reveals centromeric chromatin stability, size, and cell cycle mechanisms to maintain centromere homeostasis. *Prog Mol Subcell Biol* 56: 139 – 162

Stellfox ME, Nardi IK, Knippler CM, Foltz DR (2016) Differential binding partners of the Mis18α/β YIPPEE domains regulate Mis18 complex recruitment to centromeres. *Cell Rep* 15: 2127 – 2135

Sugimoto K, Yata H, Muro Y, Himeno M (1994) Human centromere protein C (CENP-C) is a DNA-binding protein which possesses a novel DNA-binding motif. *J Biochem* 116: 877 – 881

Sullivan BA, Karpen GH (2004) Centromeric chromatin exhibits a histone modification pattern that is distinct from both euchromatin and heterochromatin. *Nat Struct Mol Biol* 11: 1076 – 1083

Sullivan BA (2010) Optical mapping of protein-DNA complexes on chromatin fibers. *Methods Mol Biol* 659: 99 – 115

Sullivan LL, Boivin CD, Mravinac B, Song IY, Sullivan BA (2011) Genomic size of CENP-A domain is proportional to total alpha satellite array size at human centromeres and expands in cancer cells. *Chromosome Res* 19: 457 – 470

Suzuki N, Nakano M, Nozaki N, Egashira S-I, Okazaki T, Masumoto H (2004) CENP-B interacts with CENP-C domains containing Mif2 regions responsible for centromere localization. *J Biol Chem* 279: 5934 – 5946

Swartz SZ, McKay LS, Su K-C, Bury L, Padeganeh A, Maddox PS, Knouse KA, Cheeseman IM (2019) Quiescent cells actively replenish CENP-A nucleosomes to maintain centromere identity and proliferative potential. *Dev Cell* 51: 35 – 48.e7

Tachiwana H, Miya Y, Shono N, Ohzeki J-I, Osakabe A, Otake K, Larionov V, Earnshaw WC, Kimura H, Masumoto H *et al* (2013) Nap1 regulates proper CENP-B binding to nucleosomes. *Nucleic Acids Res* 41: 2869 – 2880

Tokunaga M, Imamoto N, Sakata-Sogawa K (2008) Highly inclined thin illumination enables clear single-molecule imaging in cells. *Nat Methods* 5: 159 – 161

Voullaire LE, Slater HR, Petrovic V, Choo KH (1993) A functional marker centromere with no detectable alpha-satellite, satellite III, or CENP-B protein: activation of a latent centromere? *Am J Hum Genet* 52: 1153 – 1163

Wang J, Liu X, Dou Z, Chen L, Jiang H, Fu C, Fu G, Liu D, Zhang J, Zhu T *et al* (2014) Mitotic regulator Mis18β interacts with and specifies the centromeric assembly of molecular chaperone holliday junction recognition protein (HJURP). *J Biol Chem* 289: 8326 – 8336

Weir JR, Faesen AC, Klare K, Petrovic A, Basilico F, Fischböck J, Pentakota S, Keller J, Pesenti ME, Pan D *et al* (2016) Insights from biochemical reconstitution into the architecture of human kinetochores. *Nature* 537: 249 – 253

Xiao H, Wang F, Wisniewski J, Shaytan AK, Ghirlando R, FitzGerald PC, Huang Y, Wei D, Li S, Landsman D *et al* (2017) Molecular basis of CENP-C association with the CENP-A nucleosome at yeast centromeres. *Genes Dev* 31: 1958 – 1972

Xu T, Park SK, Venable JD, Wohlschlegel JA, Diedrich JK, Cociorva D, Lu B, Liao L, Hewel J, Han X *et al* (2015) ProLuCID: an improved SEQUEST-like algorithm with enhanced sensitivity and specificity. *J Proteomics* 129: 16 – 24

Yang CH, Tomkiel J, Saitoh H, Johnson DH, Earnshaw WC (1996) Identification of overlapping DNA-binding and centromere-targeting domains in the human kinetochore protein CENP-C. *Mol Cell Biol* 16: 3576 – 3586

Zasadzińska E, Foltz DR (2017) Orchestrating the specific assembly of centromeric nucleosomes. *Prog Mol Subcell Biol* 56: 165 – 192

Expanded View Figures

Figure EV1. (related to Fig 1). *De novo* CENP-A reloading follows the canonical CENP-A deposition pathway.

A Image of IAA-treated cells. IAA escaper is highlighted with a dashed yellow circle, and CENP-A depleted cells are contoured with red dashed lines. Scale bar, 10 μm.
B Schematic for the experiments shown in C.
C Quantification of centromeric CENP-A levels normalized to non-treated level. Each dot represents one experiment, and error bars represent SD. Unpaired *t*-test: $*P = 0.0493$.
D Quantification of the relative number of DLD-1 (square) and U-2OS (circle) cells with centromeric CENP-A at the indicated timing of IAA treatment and recovery. Each dot represents one experiment with at least 20 cells per condition. Error bars represent standard deviation (SD) from 3 independent experiments.
E Schematic for the experiments shown in F-H.
F Left panel: representative images to confirm M18BP1 knock-down in late M phase cells. Scale bar, 10 μm. Yellow dashed lines highlight nuclei of daughter cells. Right panel: relative M18BP1 levels in late M/early G1 phase after siRNA knock-down using M18BP1 antibody. Each dot represents one centromere, and error bars represent standard deviation.
G Representative images of *de novo* CENP-A reloading upon M18BP1 knock-down. Nuclei are highlighted with white dashed lines. Scale bar, 5 μm.
H Quantification of centromeric CENP-A intensities in the indicated conditions (relative intensities normalized to CENP-A level in untreated cells). Each dot represents one experiment (> 30 cells per condition per experiment), and error bars represent SD of 2 independent experiments.
I Schematic representation for the experiments shown in J-K.
J Bar graphs showing quantification of centromeric CENP-A intensities following the indicated treatment. Each dot represents one experiment with at least 30 cells. Error bars represent SD of 2 independent experiments.
K Immunoblot of total protein levels in the indicated cell lines and conditions.

Source data are available online for this figure.

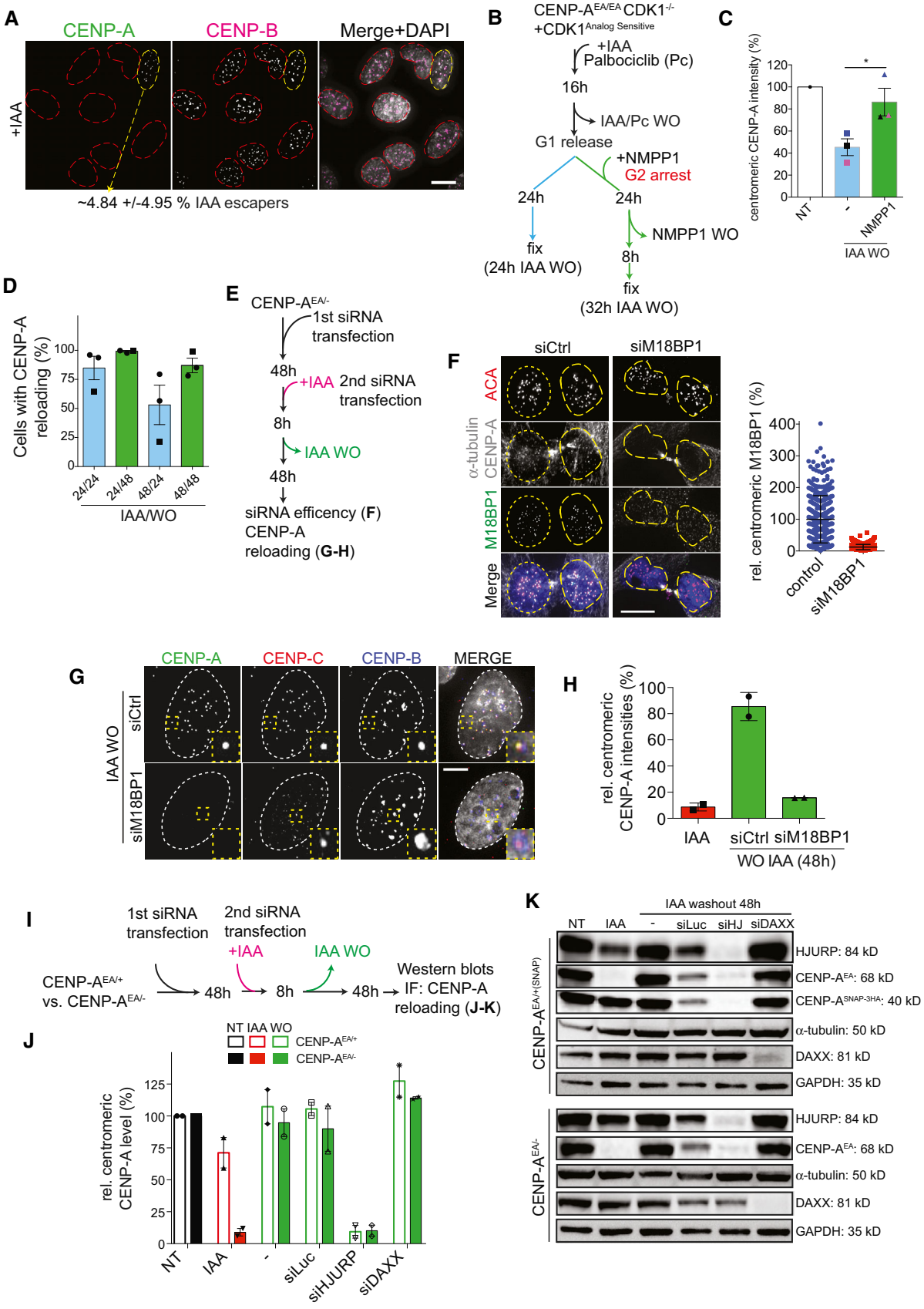

Figure EV1.

Figure EV2. (related to Fig 2). Complete centromeric CENP-A^{EA} depletion with the AID system.

A Schematic illustration of experiment shown in B, C.

B Representative images showing complete depletion of CENP-A^{EA} despite doxycycline (DOX)-induced overexpression in DLD-1 cells. Nuclei are contoured with white dashed lines. Scale bar, 5 μm.

C Quantification of CENP-A intensities in the nucleus and at the centromere in the presence or absence of IAA/DOX. Endogenous (End.) CENP-A$^{EYFP\text{-}AID}$ (CA) or overexpressed (OE) CA is depleted to non-detectable background-level in the presence of IAA. Each dot represents a cell. Mean CA intensities are indicated by a black line.

D Schematic illustration of the single molecule microscopy (SMM) experiments shown in E, G.

E Representative microscopy images from live cell imaging and corresponding 3D surface plots showing single molecule GR^{EYFP} detection in I and following IAA treatment CENP-A^{EA} signal absence at CENP-B^{mcherry} marked centromeres in II, using SMM acquisition settings.

F Examples of background-corrected EYFP signal intensities quantified over time (as shown in D) for single GR^{EYFP} molecules (in magenta), centromeric EYFP signals in IAA-treated CENP-A$^{EA/EA}$ cells (in green), and in the absence of EYFP molecules (in black).

G Signal quantification as shown in D in the indicated conditions. Unpaired *t*-test, ns ($P = 0.88$), ****$P < 0.0001$, error bars represent standard deviation. Each dot represents the quantification of one GR^{EYFP} signal (GR^{EYFP}, $n = 13$) or one centromere, respectively (No EYFP CENP-C^{mcherry}, $n = 85$ and CENP-B^{mcherry} CENP-A^{EA}, $n = 52$).

H CENP-A levels at the indicated HOR arrays quantified by CUT&RUN sequencing. CENP-A levels 48 h after IAA wash-out recover at the original HOR.

I Quantifications of CENP-A occupancy at the DXZ1 HOR array after one CENP-A$^{OFF/ON}$ cycle in DLD-1 cells using IF-FISH on chromatin fibers. Each dot represents a single chromatin fiber. Error bars show standard deviation. *P*-values from unpaired *t*-test.

J Line scan analysis at the D7Z1 array on chromosome spreads in the indicated treatment. Scale bar, 2 μm.

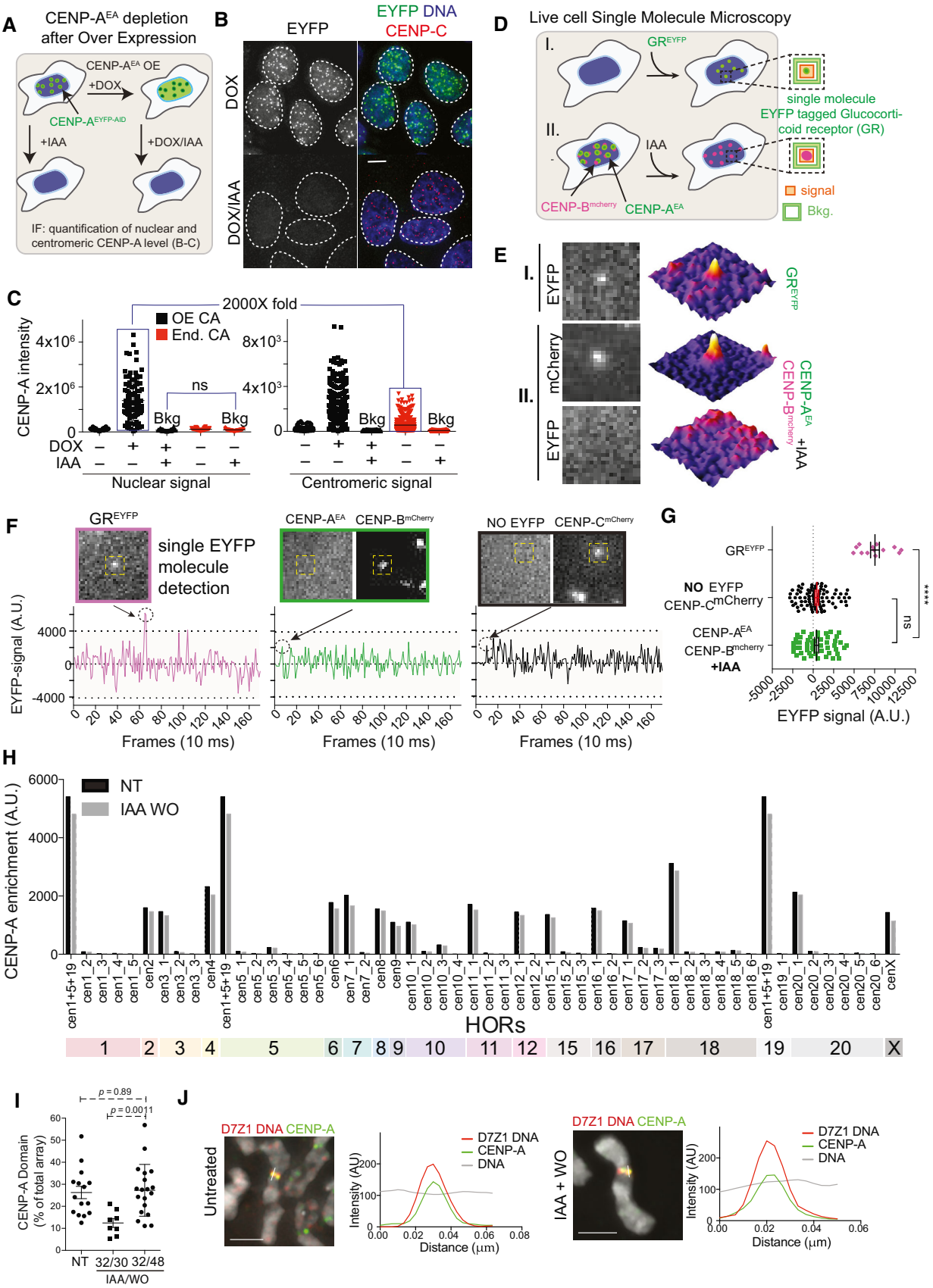

Figure EV2.

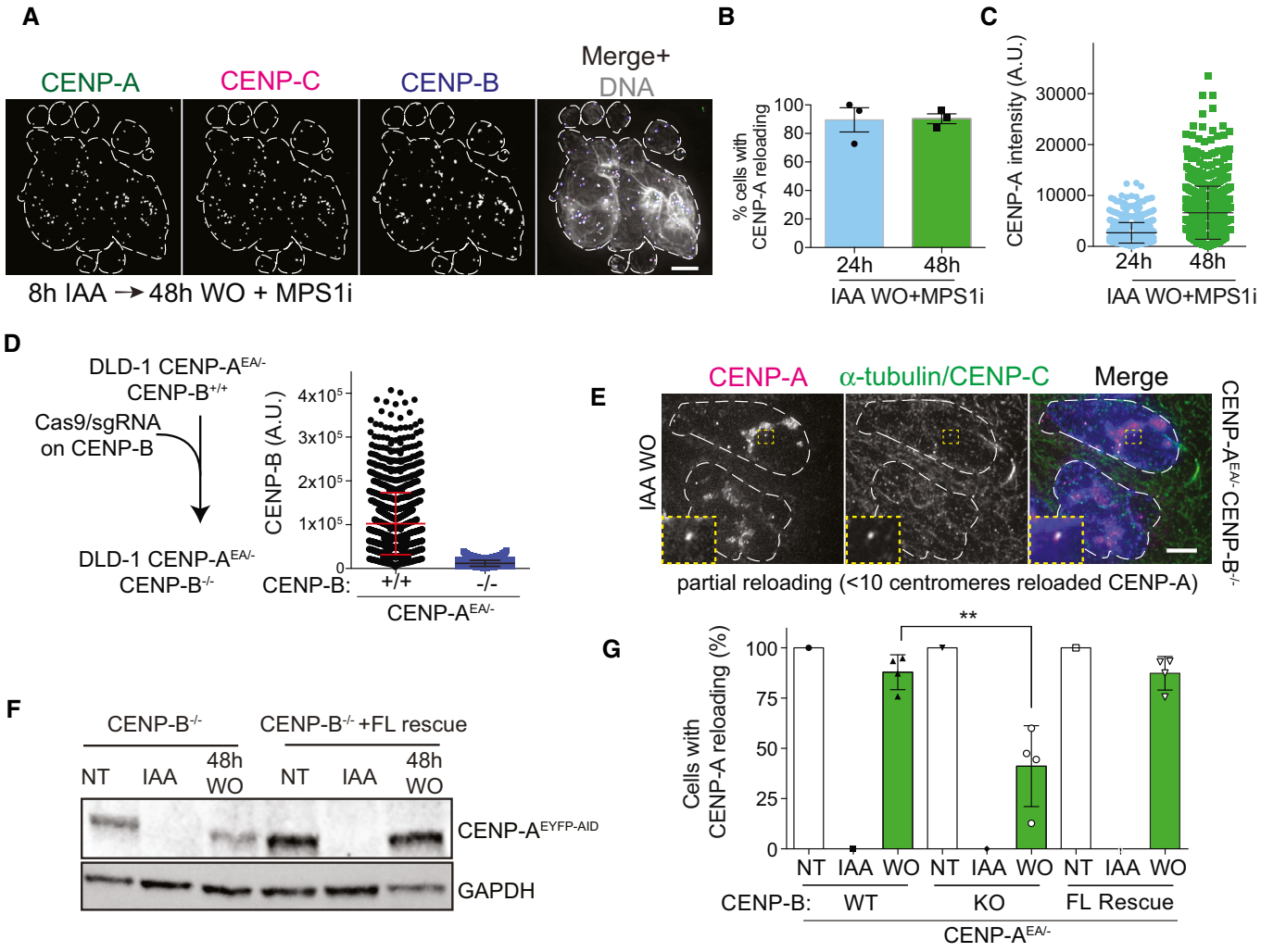

Figure EV3. (related to Fig 3). CENP-B is a key factor for efficient *de novo* CENP-A reloading.

A Representative immunofluorescence showing *de novo* CENP-A deposition in CENP-B (+/+) DLD-1 cells after reversine-induced chromosome mis-segregation. DAPI staining is contoured by a white dashed line. Scale bar, 5 μm.

B, C Bar graphs showing the relative number of CENP-A-positive cells (B) and the level of centromeric CENP-A level (C) in the presence of reversine. Each dot represents one experiment with more than 20 cells per condition. Error bars represent SD of 3 independent experiments.

D Left: schematic of the CRISPR/Cas9 strategy to deplete CENP-B in DLD-1 cells as measured in the dot plot on the right. Each dot represents one centromere, and error bars show standard deviation.

E Immunofluorescence images showing partial *de novo* CENP-A^{EA} reloading (< 10 centromeres) in CENP-B$^{-/-}$ DLD-1 cells in late M phase. Nuclei of daughter cells are highlighted with white dashed lines. Scale bar, 5 μm.

F Immunoblot of total protein levels in the indicated conditions in the indicated cell line. FL = full length.

G Bar graphs showing the relative number of DLD-1 cells with centromeric CENP-A in indicated conditions in the indicated cell line. Each dot represents one single experiment, > 30 cells per condition. Unpaired *t*-test, $^{**}P$ = 0.0053, error bars represent SD of 4 independent experiments.

Source data are available online for this figure.

Figure EV4. (related to Fig 7). Exogenously expressed CENP-C, but not CENP-A, reloaded at the original centromere position in absence of endogenous CENP-A/C.

A Models of CENP-B-induced CENP-A reloading via (I.) initial Mis18 recruitment or (II.) initial CENP-C recruitment.
B Schematic of the experiment analyzed in C, D.
C Quantification of M18BP1 foci in late M phase/early G1 (eG1) in both daughter cells in the indicated conditions. Each dot represents two daughter cells. Error bars show SEM. Unpaired *t*-test: ****$P < 0.0001$.
D Representative immunofluorescence images showing M18BP1 foci in different cell lines after 24-h IAA treatment. Cells with centromeric CENP-A are marked with a red dashed contour line, while a yellow contour line marks cell without centromeric CENP-A. Scale bar, 5 μm.
E Illustration of the genomic make-up of DLD-1 cells used to test CENP-A or CENP-C reloading in the absence of endogenous CENP-A/C.
F Immunoblot showing exogenous CENP-A (left) and CENP-C (right) expression upon addition of doxycycline (DOX) and TMP to induce CENP-$A^{DHFR\text{-}mRFP}$ or CENP-$C^{DHFR\text{-}mRFP}$ overexpression in DLD-1 cells.
G Experimental design of experiments shown in Fig 7C–E and Appendix Fig S7H and I.
H Bar graphs showing the control of CUT&RUN–qPCR on CENP-C antibody and primers binding to the centromere of chromosome 4 in the indicated conditions. Enrichment is measured relative to the IgG control and normalized to Alu repeats. Error bars represent SD of 3 independent experiments.
I Representative immunofluorescence image showing 24 h CENP-$A^{mRFP\text{-}DHFR}$ stability in the absence of endogenous CENP-A and CENP-C in G1 arrested cells.
J Experimental design of experiments shown in Fig 7F–H and Appendix Fig S7K–M.
K Representative immunofluorescence image showing CENP-C reloading in interphase cells (nuclei are highlighted by a dashed red contour line) in the presence (control) or absence (sample) of endogenous CENP-A/C. Scale bar, 5 μm.
L Quantification of relative number of exogenous CENP-C-positive centromeres per cell in the indicated conditions quantified on chromosome spreads.
M Bar graph showing the control of CUT&RUN–qPCR on CENP-A antibody and primers binding to the centromere of chromosome 4 in the indicated conditions. Enrichment is measured relative to the IgG control and normalized to Alu repeats.

Source data are available online for this figure.

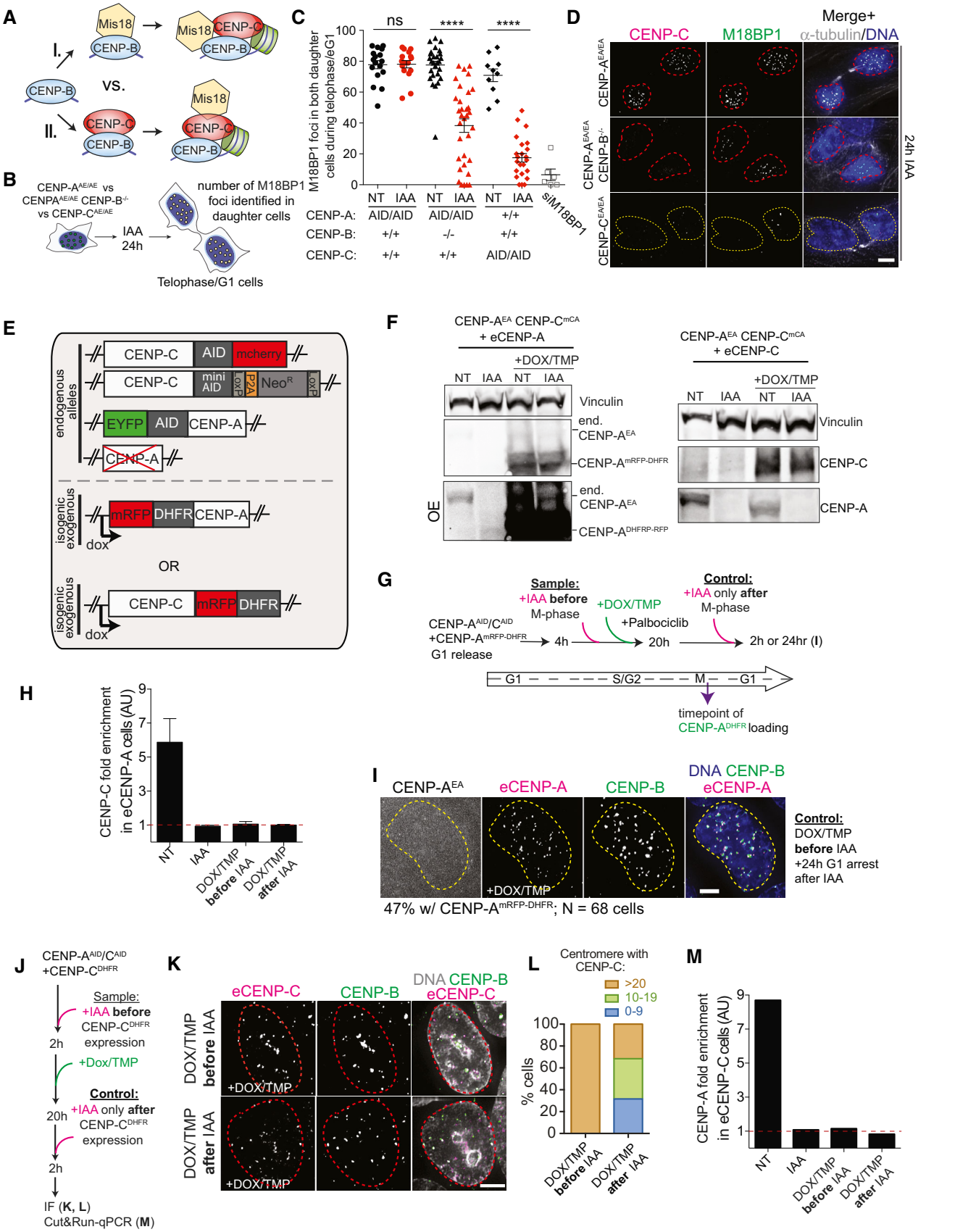

Figure EV4.

Figure EV5. (related to Fig 8). CENP-A-deprived CD4$^+$ T cells are found in human blood samples but disappear upon T-cell activation.

A Representative FACS plots showing the efficiency of total CD4$^+$ T-cell purification from human blood PBMCs.

B Representative FACS plots showing gating of CENP-B-positive/CENP-A-high and CENP-B-positive/CENP-A-low populations of freshly purified human CD4^{+z} T cells based on isotype controls. Ms = mouse; Rb = rabbit.

C Graph showing CENP-A foci identified in high or low CENP-A expressing cell colocalizing with CENP-B foci in two donors. Each dot represents the percentage of CENP-A/B colocalizing in one cell. Error bar shows SEM.

D Quantification of centromeric CENP-A level in high or low CENP-A expressing CD4$^+$ T cells. Each dot represents one centromere. Error bars show standard deviation.

E Representative immunofluorescence images showing CENP-B- and CENP-C-positive centromeres, but lacking CENP-A in a CD4$^+$ T cell. Nucleus is contoured by a dashed yellow line. Scale bar, 5 μm

F Representative plots showing CENP-A expression vs. forward scatter area (FSC-A), which determines the relative size of CD4$^+$ T cells after activation. Gates represent the frequency of CENP-A high and low populations in total CD4$^+$ T (shaded gates represent CENP-A^{low} cells).

G Graph representing the absolute number of CFSE-high/CENP-A-low CD4$^+$ T cells during the experimental kinetics. One-way ANOVA, multiple comparisons, $n = 6$ (each symbol represents a different donor). $^{**}P < 0.01$, $^{***}P < 0.001$.

H Graph showing the frequency of dead cells in CD4$^+$ T cell cultures over time. One-way ANOVA, multiple comparisons, $n = 6$ (each symbol represents a different donor). Error bars show SEM. $^{*}P < 0.05$

I CFSE dilution and CENP-A expression at day 3 post-activation. Representative FACS plots showing CENP-A expression in CD4$^+$ T cells that have not divided (div 0) and those that have divided once or more times (div ≥ 1), gated based on CFSE dilution. Gates in CENP-A plots were set based on isotype control for each specific population (cells in shaded gates are CENP-A-low CD4$^+$ T cells).

J Graph representing the frequency of CENP-A low cells (shaded gate in I). One-way ANOVA, multiple comparisons, $n = 6$ (each symbol represents a different donor). Error bars show SEM. $^{****}P < 0.0001$.

K Representative immunofluorescence images showing CENP-A, CENP-C, and CD4 staining after FACS. Cells with centromeric CENP-A are marked with a red dashed contour line, while a yellow contour line marks cell without centromeric CENP-A. Scale bar, 5 μm.

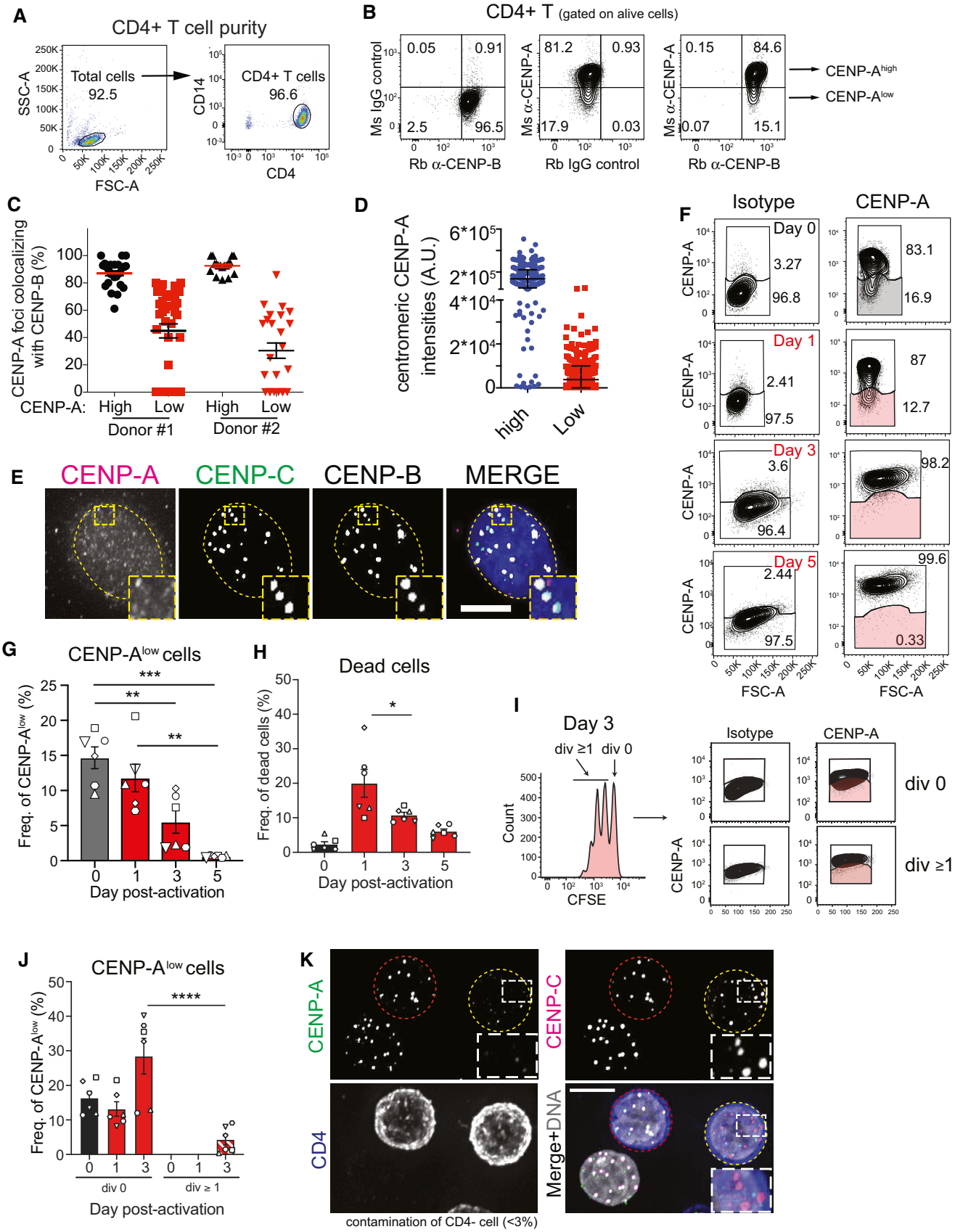
A
CD4+ T cell purity
Total cells
92.5
SSC-A
FSC-A
CD4+ T cells
96.6
CD14
CD4
B
CD4+ T (gated on alive cells)
Ms IgG control
Rb α-CENP-B
0.05
0.91
2.5
96.5
Ms α-CENP-A
Rb IgG control
81.2
0.93
17.9
0.03
0.15
84.6
0.07
15.1
CENP-A^high
CENP-A^low
C
CENP-A foci colocalizing with CENP-B (%)
CENP-A: High Low High Low
Donor #1
Donor #2
D
centromeric CENP-A intensities (A.U.)
high
Low
E
CENP-A
CENP-C
CENP-B
MERGE
F
Isotype
CENP-A
Day 0
3.27
96.8
83.1
16.9
Day 1
2.41
97.5
87
12.7
Day 3
3.6
96.4
98.2
Day 5
2.44
97.5
99.6
0.33
CENP-A
FSC-A
G
CENP-A^low cells
Freq. of CENP-A^low (%)
Day post-activation
H
Dead cells
Freq. of dead cells (%)
Day post-activation
I
Day 3
div ≥1
div 0
Count
CFSE
Isotype
CENP-A
div 0
div ≥1
J
CENP-A^low cells
Freq. of CENP-A^low (%)
div 0
div ≥ 1
Day post-activation
K
CENP-A
CENP-C
CD4
Merge+DNA
contamination of CD4- cell (<3%)

Figure EV5.